Robert J Ewart, Felix I Parra, Alessandro Geraldini

Sheath collapse at critical shallow angle due to kinetic effects

Sheath collapse at critical shallow angle due to kinetic effects

Robert J Ewart, Felix I Parra, Alessandro Geraldini

Sheath collapse at critical shallow angle due to kinetic effects

Robert J Ewart[1], Felix I Parra[1,2], Alessandro Geraldini[3,4]

[1] Rudolf Peierls Centre for Theoretical Physics, University of Oxford, Oxford, OX1 3PU, UK

[2] CCFE - UKAEA, Culham Science Centre, Abingdon OX14 3DB, UK

[3] Swiss Plasma Center, École Polytechnique Fédérale de Lausanne, CH-1015 Lausanne, Switzerland

[4] Institute for Research in Electronics and Applied Physics, University of Maryland, College Park, MD 20742 USA

E-mail: `robert.ewart@balliol.ox.ac.uk`

Abstract. The Debye sheath is shown to vanish completely in magnetised plasmas for a sufficiently small angle between the magnetic field and the wall that depends on the current to the wall. When the Debye sheath vanishes, there is still a potential drop between the wall and the plasma across the magnetic presheath. The magnetic field angle corresponding to sheath collapse is shown to be much smaller than previous estimates, scaling with the electron-ion mass ratio and not with the square root of the mass ratio. This is shown to be a consequence of the finite ion orbit width effects, which are not captured by fluid models. The wall potential with respect to the bulk plasma at which the Debye sheath vanishes is calculated. Above this wall potential, it is possible that the Debye sheath will invert.

1. Introduction and orderings

At the boundary between plasmas and absorbing surfaces, non-neutral layers, called sheaths, are known to form [1–3]. The nature of these sheaths is controlled by the difference between ion and electron mobility and the physics of their interaction with the wall. Plasma wall interaction is of great importance in many devices such as spacecrafts [4], Hall thrusters [5], plasma probes [6,7] and magnetic filters [8]. It is of particular importance for magnetic confinement fusion, where fluxes of electrons and ions from the plasma are directed by magnetic fields onto the divertor or limiter targets, which can lead to overheating and damage [9]. In order to reduce damage
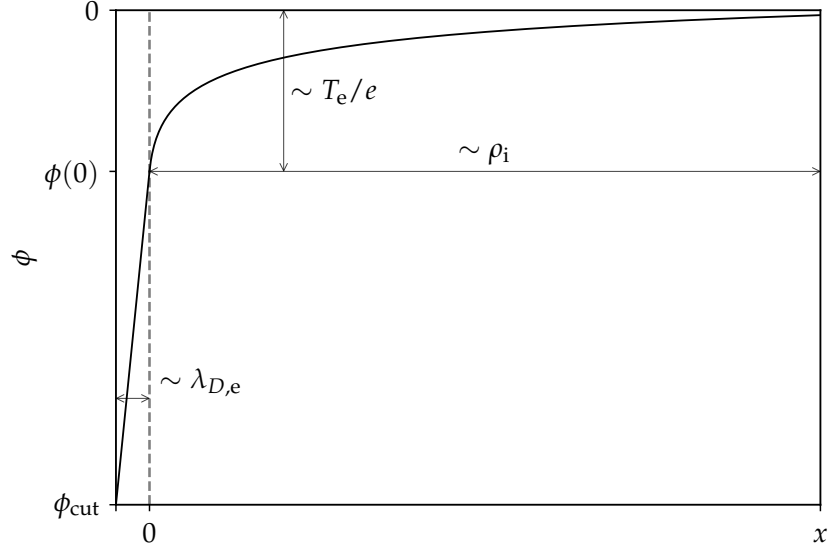
Figure 1: A cartoon of the potential profile within the magnetic presheath and the Debye sheath.

to solid targets, a common method is to incline the magnetic field at a small angle, α, relative to the wall, thus spreading heat flux over a larger area [10].

In this paper we consider the effect of magnetisation on the plasma-wall interaction. We focus on the magnetic presheath, a quasineutral layer with a size on the order of the ion gyroradius that appears on top of the typically much thinner Debye sheath in magnetised plasmas [11]. Within the magnetic presheath, we assume that the magnetic field is at a small angle α to the plane parallel to the wall of the device,

$$\mathbf{B} = -\sin\alpha\hat{\mathbf{e}}_x + \cos\alpha\hat{\mathbf{e}}_z. \tag{1}$$

Here we are using a set of orthonormal coordinates, $\{\hat{\mathbf{e}}_x, \hat{\mathbf{e}}_y, \hat{\mathbf{e}}_z\}$, such that $\hat{\mathbf{e}}_x$ points in the direction perpendicular to the wall and $\hat{\mathbf{e}}_z$ points in the direction of the component of $\mathbf{B}$ parallel to the wall. The electric field is electrostatic and points solely in the x direction, such that

$$\mathbf{E} = -\nabla\phi = -\frac{\mathrm{d}\phi(x)}{\mathrm{d}x}\hat{\mathbf{e}}_x, \tag{2}$$

where ϕ is the electrostatic potential. There is assumed to be no dependence on the

y or z coordinates and no time dependence.

The first treatment of the magnetic presheath was due to Chodura [11, 12]. This initial study used fluid equations to describe the electrons and ions, complemented by numerical simulations with a "particle-in-cell" kinetic model. Chodura found a solution to the potential throughout the presheath and a condition on the entrance ion distribution function, known as the Chodura condition, for the existence of this solution. The Chodura condition specifies that the fluid speed of ions entering the presheath along the magnetic field lines must be at least equal to the Bohm speed v_B,

$$v_B = \sqrt{\frac{ZT_e}{m_i}}, \tag{3}$$

where Z is the ion charge number, T_e is the electron temperature and m_i the ion mass. Between the magnetic presheath and the wall lies the Debye sheath. The Debye sheath has a typical thickness of several Debye lengths and, unlike the magnetic presheath, is not expected to be quasineutral. Analogous to (and predating) the Chodura condition, the Debye sheath has a 'Bohm condition' [13], which states that ions entering the Debye sheath must be moving at least at the Bohm speed towards the wall (in contrast to along the field line).

Subsequent fluid treatments of the magnetic presheath have built upon the work of Chodura. Fluid treatments are, however, only well motivated if the ion temperature T_i is much less than the electron temperature T_e [14–16]. For ion temperatures comparable to the electron temperature, the strong distortion of the ion orbits means that an accurate description of the the presheath requires a kinetic treatment. The difficulty of kinetic theory and the complication of an absorbing boundary has meant that most approaches have been numerical, with further particle-in-cell simulations and Eulerian-Vlasov codes [17–21], although some analytical progress has been made [22–24]. This paper will build on the recent work of Geraldini et al [14–16], whose kinetic model of the ions takes into account not only the distortion of the ion orbits, but also the contribution of ions that have recently broken free from their orbits due to the strong electric field near the Debye sheath. The electron density assumed by Geraldini et al, and a swathe of the literature, is Boltzmann distributed. This model is, in general, only valid in the limit of a very large potential drop in the Debye sheath, when most electrons are reflected. A common model to give the electrons a net flux is to truncate the entrance electron distribution in the velocity component along the magnetic field line [25–27]. The

truncation velocity is determined by the wall potential because electrons considered energetic enough to reach the wall are assumed to be absorbed instead of reflected. In this paper, we will provide a drift kinetic derivation for such a model. We will treat the wall potential as a parameter, denoted ϕ_{cut}, referred to as the 'cutoff potential' or simply the 'cutoff'. It is assumed that the potential and its first two derivatives are monotonic converging to zero as $x \to \infty$ throughout this paper. Therefore, the imposed cutoff potential also sets a lower bound for the potential throughout the magnetic presheath. However, this lower bound is not usually reached within the presheath. Indeed, when the potential in the presheath does not reach the cutoff potential, this implies the remainder of the potential drop occurs in the Debye sheath (see figure 1).

The width of the presheath will be set by the distance at which ion orbits begin to contact the wall, which is of the order the ion gyroradius, ρ_{i}. The potential drop must be sufficient to repel a considerable fraction of the electrons. Hence, we arrive at the following ordering for the potential and its first derivative,

$$\phi(x) \geq \phi_{\mathrm{cut}} \sim \frac{T_{\mathrm{e}}}{\mathrm{e}} \tag{4}$$

and

$$\frac{\mathrm{d}\phi}{\mathrm{d}x} \sim \frac{T_{\mathrm{e}}}{\mathrm{e}\rho_{\mathrm{i}}}. \tag{5}$$

One could imagine having a dial on the wall of the device that controlled the cutoff potential. Cutoffs corresponding to energies much greater than the electron thermal energy would result in only very fast electrons reaching the wall, of which there will be exponentially few. As such, it is cutoffs at ordering (4) that we expect to significantly alter the electron distribution function.

The typical velocity of electrons is ordered as

$$|\mathbf{v}_{\mathrm{e}}| \sim v_{\mathrm{t,e}} = \sqrt{\frac{2T_{\mathrm{e}}}{m_{\mathrm{e}}}}, \tag{6}$$

and the typical velocity of ions as

$$|\mathbf{v}_{\mathrm{i}}| \sim \sqrt{\frac{ZT_{\mathrm{e}} + T_{\mathrm{i}}}{m_{\mathrm{i}}}}. \tag{7}$$

Throughout this article we will use an 'i' subscript to refer to quantities associated with the ions and an 'e' subscript for the electrons. When we wish to refer to both electrons and ions we will use the subscript 's' for species.

Due to the Bohm and Chodura conditions, the fluid velocity of the ions in the x direction must become more negative as we approach the wall: the potential drop accelerates the ions towards the wall. By conservation of particle flux, the density must therefore decrease. This allowed Chodura to arrive at his prediction for the ion density at the Debye sheath entrance of [11]

$$n_i(0) = \alpha n_{i,\infty},\tag{8}$$

where $n_{i,\infty}$ is the ion density at $x \to \infty$. Since the system is quasineutral and the densities are approximately Boltzmann related ($n_e \approx n_{e,\infty} \exp(e\phi/T_e)$), the corresponding potential drop in the presheath is

$$\frac{e\phi(0)}{T_e} = \ln \alpha.\tag{9}$$

Typical estimates of the total potential drop (ϕ_{cut} in our notation) over the presheath and Debye sheath come from considering the case of an electrically floating wall accepting equal and opposite electron and ion currents. The typical scaling of such cutoff potentials was found to be [9, 11, 28]

$$\frac{e\phi_{\text{cut}}}{T_e} = \frac{1}{2} \ln \left(\frac{m_e}{m_i} g \left(\frac{T_i}{T_e} \right) \right).\tag{10}$$

Here g is a function of the ion to electron temperature ratio T_i/T_e which is independent of α. The important feature of this scaling for the total potential drop is its dependence on mass ratio and its lack of α dependence. Stangeby [28] noted that, for sufficiently shallow magnetic field angle, the potential drop in the presheath predicted by Chodura could equal or exceed the total potential drop in the combined presheath and Debye sheath. This would imply that there is a magnetic field angle at which the Debye sheath would collapse. By direct comparison of equations (9) and (10), Stangeby predicted sheath collapse at an angle that scales as the square root of mass ratio and had value $3.35°$ for a deuterium plasma. This prediction for sheath collapse provides a relevant ordering for the smallness of α, given by

$$\alpha = O \left(\sqrt{\frac{m_e}{m_i}} \right).\tag{11}$$

The assumptions that led to this ordering for sheath collapse are, however, incorrect as they fail to account for the alteration to Chodura's fluid model due to the loss of

electrons onto the wall and the resulting breakdown of the assumption of Boltzmann electrons. We will prove that, in fact, there is no Debye sheath collapse for the fluid model. Stangeby's central idea that an increasing potential drop across the presheath can cause the Debye sheath to collapse, is nonetheless correct, but in fact this collapse owes its origins to finite ion orbit widths and is therefore an intrinsically kinetic effect. Furthermore, we will show that it occurs at angles which scale linearly with mass ratio, much smaller than those predicted by Stangeby.

The discrepancy can be understood by first noting that equation (8) for the drop in density in the presheath is incorrect when the electric field only weakly distorts ion orbits, which is exactly the case when the Debye sheath vanishes. When the ions are only weakly distorted by the electric field, their near-circular orbits give rise to a density at the wall (or equivalently the Debye sheath entrance) that scales like $\alpha^{1/2}$, instead of like α [15,23]. To see this, we appeal to a geometrical picture of a circular orbit near the wall, shown in figure 2. Because the ions are on circular orbits, the ion reaching the wall with the largest component of velocity perpendicular to the wall is the ion that just grazed it on its previous cycle. If such an ion is moving at typical thermal velocities along the magnetic field line, in the time it takes for the ion to make a single gyration, it will have drifted closer to the wall by a distance of order $\alpha\rho_i$. The ion velocity then makes an angle θ to the wall, shown in figure 2, which we argue scales as $\sqrt{\alpha}$. This means the velocity onto the wall scales as $\sqrt{\alpha}v_{t,i}$. Since the ion flux at infinity scales like $\alpha v_B n_{i,\infty}$, by particle flux conservation, the density at the wall must scale like $\sqrt{\alpha}n_{i,\infty}$. We will prove this scaling algebraically in section 2.3, but this simplified picture serves to gain an estimate and also shows why this could not be predicted by a fluid model.

Equipped with this estimate for the ion density, we see that the new estimate for the potential drop in the presheath is

$$\frac{e\phi(0)}{T_e} = O\left(\frac{1}{2}\ln\alpha\right). \tag{12}$$

Direct comparison between equations (12) and (10) now implies that the Debye sheath will vanish at an angle α that scales with mass ratio rather than square root mass ratio. This motivates a different, smaller, ordering for α, given by

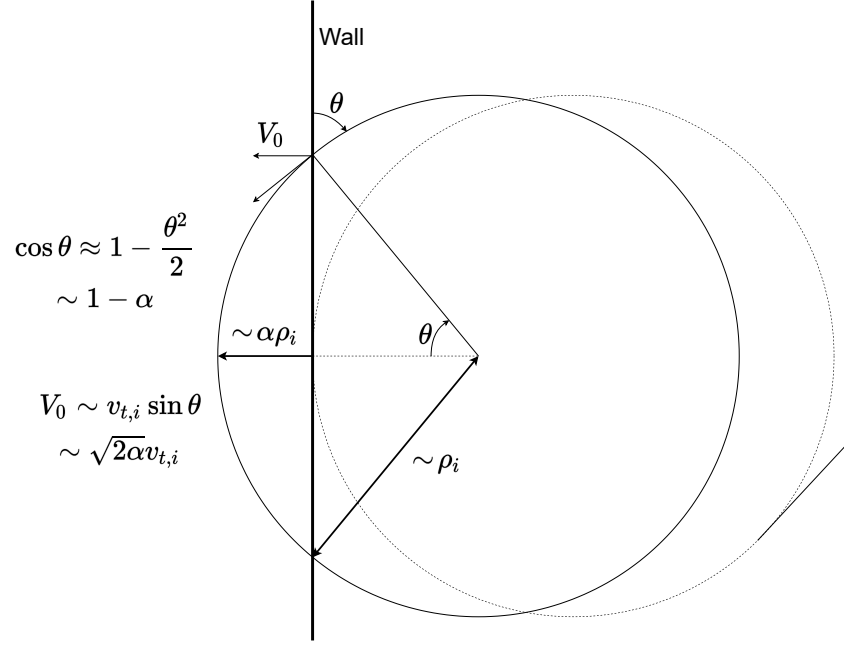$$\alpha = O\left(\frac{m_e}{m_i}\right). \tag{13}$$

Figure 2: A sketch of a circular ion orbit drifting towards the wall. The ions approaching the wall with the largest velocity perpendicular to the wall are those that just grazed the wall on the previous gyration (dashed line). In a time $\sim 1/\Omega_i$ the ion orbit drifts a distance $\alpha\rho_i$ towards the wall, causing these ions to make an angle of order $\sqrt{\alpha}$ to the wall. The angles in this diagram have been exaggerated for clarity.

The rest of the paper is structured as follows. In section 2 we will discuss the single particle motion of electrons and ions within the presheath, showing both to be quasi-periodic. We will build on this idea in subsections 2.2 and 2.3, developing a model for the electron distribution function within the presheath and reviewing the model developed in [14, 15] for the ions. To correctly capture the physics of sheath collapse, we ensure that our electron model is valid in both the previously predicted ordering for collapse (equation (11)), and our revised smaller ordering (equation (13)). In section 3 we will use the ion and electron models to derive expressions for the density within the presheath accounting for electrons absorbed onto the wall. In section 4 we will expand the quasineutrality equation close to and far from the wall analytically. Far from the wall, this will give rise to the modified

kinetic Chodura condition, while close to the wall we will prove that, for the majority of the solutions, the presheath will satisfy a marginal kinetic Bohm condition. The truncation of the electron distribution will lead to a subsonic Bohm condition, which agrees qualitatively with the predictions of [28]. In order to gain insight into these specific solutions, we will appeal to the limits of hot and cold ion temperatures in section 5. We will see that there exist cutoff potentials that do not admit solutions, and that this lack of solutions is tied to finite orbit effects. These effects manifest themselves most obviously in the hot ion limit. We will show they are not present in the limit of cold ions. In section 6 we will detail how our solutions are reached numerically and where this procedure differs from [15]. In section 7 we will show our numerical solutions to the presheath for a range of temperature ratios, angles α, and cutoff potentials. We will show that there are indeed ranges of cutoffs for which no solution exists. Furthermore, we will show that this lack of solutions implies that there are angles of the magnetic field for which the current from the plasma cannot be zero unless the electric field of the Debye sheath reverses. This sheath reversal happens for angles α of order m_e/m_i.

2. Trajectories within the presheath

In this section we will discuss the models that we use for the electron and ion orbits within the presheath. This will begin with a brief discussion of the constants of the motion at $\alpha = 0$ and a justification of treating the electron and ion motion as periodic. In subsection 2.2 we exploit the smaller electron orbits to simplify the electron equations of motion. In subsection 2.3 we will review the formalism presented in [15] to find the ion density in the presheath for a given potential profile.

2.1. The $\alpha = 0$ problem and quasi-periodicity

The equations of motion for ions and electrons in the presheath are

$$\dot{v}_x = -\text{sgn}(Z_s)\frac{\Omega_s}{B}\frac{\mathrm{d}\phi}{\mathrm{d}x} + \text{sgn}(Z_s)\Omega_s v_y \cos\alpha, \tag{14}$$

$$\dot{v}_y = -\text{sgn}(Z_s)\Omega_s v_x \cos\alpha - \text{sgn}(Z_s)\Omega_s v_z \sin\alpha, \tag{15}$$

and

$$\dot{v}_z = \text{sgn}(Z_s)\Omega_s v_y \sin\alpha. \tag{16}$$

Here $\Omega_s = |Z_s|eB/m_s$ is the gyrofrequency of a particular species. The factors of $\text{sgn}(Z_s)$ have appeared so we may refer to Ω_s as a positive quantity for electrons and ions.

The trajectories defined by equations (14-16), as in [14, 15], can be solved for $\alpha = 0$, giving the constants of the motions $U_\perp$, U and $\bar{x}$ defined by

$$\bar{x} = x + \text{sgn}(Z_s)\frac{v_y}{\Omega_s}, \tag{17}$$

$$U_\perp = \frac{1}{2}v_x^2 + \frac{1}{2}v_y^2 + \text{sgn}(Z_s)\frac{\Omega_s\phi}{B}, \tag{18}$$

and

$$U = \frac{1}{2}v_x^2 + \frac{1}{2}v_y^2 + \frac{1}{2}v_z^2 + \text{sgn}(Z_s)\frac{\Omega_s\phi}{B}. \tag{19}$$

Here $\bar{x}$ is a constant of the motion that will later be useful for characterising orbits, and $U_\perp$ and U are the perpendicular and total energy, respectively. For $\alpha \neq 0$, $\bar{x}$ and $U_\perp$ are no longer constants of the motion. In this case we take equations (17) and (18) to be the definitions of these quantities, with the understanding that they are no longer constants of the motion. Indeed, we may now use our equations of motion to determine the rates of change of $\bar{x}$ and $U_\perp$,

$$\dot{\bar{x}} = -v_z\alpha + O(v_{t,s}\alpha^2), \tag{20}$$

and

$$\dot{U}_\perp = -\text{sgn}(Z_s)\Omega_s v_z v_y\alpha + O(v_{t,s}^2\alpha^3). \tag{21}$$

Hence, while $\bar{x}$ and $U_\perp$ are no longer constants of the motion for $\alpha \neq 0$, they are still useful as they vary slowly in α.

We may use our definition (17) to rewrite $U_\perp$ as

$$\begin{aligned}
U_\perp &= \frac{1}{2}v_x^2 + \frac{1}{2}\Omega_s^2(\bar{x} - x)^2 + \text{sgn}(Z_s)\frac{\Omega_s\phi}{B} \\
&= \frac{1}{2}v_x^2 + \chi(x, \bar{x}).
\end{aligned} \tag{22}$$

Here we have defined the effective potential $\chi(x, \bar{x})$ (which will be most relevant for the ion model) as

$$\chi(x, \bar{x}) = \frac{1}{2}\Omega_s^2(\bar{x} - x)^2 + \text{sgn}(Z_s)\frac{\Omega_s}{B}\phi. \tag{23}$$

When $\alpha = 0$, $U_\perp$ and $\bar{x}$ are constants and thus the motion is truly periodic in x for certain values of $U_\perp$ and $\bar{x}$. Equation (17) implies that the range of x sampled in one period will be $\sim \rho_s = v_{t,s}/\Omega_s$ and thus the period of the motion will be $\sim 1/\Omega_s$ by equation (22). When $\alpha \neq 0$, the change in $U_\perp$ over a time $1/\Omega_s$ will be a factor of α smaller than the value of $U_\perp$ by equation (21). Hence the motion is no longer truly periodic, but we will refer to it as 'quasi-periodic' since the particles are moving in a potential well that is changing slowly compared to the time taken to cross the well.

While we have thus far used $U_\perp$ to discuss the quasi-periodic motion of the electrons and ions, it is possible, for a system with two well separated timescales, to have another variable that is constant to the desired order in the expansion parameters. Such a variable is known as an adiabatic invariant. We will give an expression for the adiabatic invariant, μ, for electrons in section 2.2.

2.2. Drift kinetic electrons

In section 2.1 we have explained that the motion of the ions and electrons is quasi-periodic for $\alpha \ll 1$. Here we focus solely on the electron model. The Vlasov equation for the evolution of the electron distribution function is

$$\frac{\partial f_e}{\partial t} + \mathbf{v} \cdot \nabla f_e - \frac{e}{m_e}\left(\mathbf{E} + \mathbf{v} \times \mathbf{B}\right) \cdot \nabla_v f_e = 0. \tag{24}$$

The aim of this section is to rewrite equation (24) to achieve an expression for how the distribution function changes as we move into the presheath. Equation (20) implies that, despite their fast oscillations with timescale $1/\Omega_e$, the electrons approach the wall on a timescale $\rho_i/v_{t,e}\alpha$. Furthermore, the electrons oscillate on length scales of order ρ_e, much smaller than the characteristic width of the presheath. We will therefore be able to expand the electron motion in small $\rho_e/\rho_i \sim \sqrt{m_e/m_i}$ as well as small angle α. Given such conditions, the classic approach to this problem is that of drift kinetics [29]. Hence we will change variables to those quantities that vary slowly over a single particle oscillation. Of course, one coordinate must still capture the fast oscillations of the electrons. This variable is the gyrophase, φ, defined by

$$\varphi = -\tan^{-1}\left(\frac{(\mathbf{v} - \mathbf{v_E}(x)) \cdot \hat{\mathbf{e}}_y}{(\mathbf{v} - \mathbf{v_E}(x)) \cdot \hat{\mathbf{e}}_n}\right) = -\tan^{-1}\left(\frac{v_y - v_E}{v_n}\right). \tag{25}$$

Here $\hat{\mathbf{e}}_n = \cos\alpha\,\hat{\mathbf{e}}_x + \sin\alpha\,\hat{\mathbf{e}}_z$ denotes the unit vector perpendicular to both the magnetic field and the y direction. The quantity $v_n = \mathbf{v} \cdot \hat{\mathbf{e}}_n$ is the component of

velocity in the direction of $\hat{\mathbf{e}}_n$ while $\mathbf{v_E}$ denotes the $\mathbf{E} \times \mathbf{B}$ drift velocity,

$$\mathbf{v_E} = \frac{1}{|\mathbf{B}|} \mathbf{E} \times \hat{\mathbf{b}} = \frac{1}{B} \frac{\mathrm{d}\phi}{\mathrm{d}x}(x) \cos \alpha \hat{\mathbf{e}}_y. \tag{26}$$

We have chosen to use velocities suited to the basis $\{\hat{\mathbf{e}}_n, \hat{\mathbf{e}}_y, \hat{\mathbf{b}}\}$ as it is in the plane perpendicular to the magnetic field that the electrons oscillate. Using this basis removes certain terms small in α that would complicate the algebra.

As shown in section 2.1, many of the possible parameters that specify the electron's position in phase space vary slowly over a single orbit. The variables we choose are U, the energy, defined by equation (19), and μ, the adiabatic invariant, defined by

$$\mu = \frac{1}{2\Omega_e} \left(|\mathbf{v} - \mathbf{v_E}(x)|^2 - |\mathbf{v} \cdot \mathbf{b}|^2 \right) = \frac{1}{2\Omega_e} \left(v_n^2 + (v_y - v_E)^2 \right). \tag{27}$$

We have chosen this variable over $U_\perp$ as it is designed to vary on average zero over a single period and is also very convenient for expressions involving φ.

Using equations (17), (19), (25), and (27), we change from $\{t, \mathbf{r}, \mathbf{v}\}$ to the new variables $\{t, \bar{x}, y, z, U, \mu, \varphi\}$. In these variables the Vlasov equation (24) becomes

$$\dot{\bar{x}} \frac{\partial f_e}{\partial \bar{x}} + \dot{\mu} \frac{\partial f_e}{\partial \mu} + \dot{\varphi} \frac{\partial f_e}{\partial \varphi} = 0, \tag{28}$$

where we have removed the t, y and z related terms as the distribution is independent of these (as explained in the introduction), and we have removed the term $\dot{U}(\partial f_e/\partial U)$ since $\dot{U} = 0$. Here, the dot operator is defined by

$$\dot{Q} = \frac{\partial Q}{\partial t} + \mathbf{v} \cdot \nabla Q - \frac{e}{m_e} \left(\mathbf{E} + \mathbf{v} \times \mathbf{B} \right) \cdot \nabla_v Q, \tag{29}$$

which we compute explicitly in Appendix A for our variables. From these, we may examine the quantity $\dot{Q}/Q$ to find the characteristic frequency of each of our variables. Equations (A.3), (A.4) and (A.5) give the scalings

$$\frac{\dot{\bar{x}}}{\rho_i} = O \left(\frac{v_{t,e}}{\rho_i} \alpha \right), \tag{30}$$

$$\frac{\Omega_e \dot{\mu}}{v_{t,e}^2} = O \left(\frac{v_{t,e}}{\rho_i} \sqrt{\frac{m_e}{m_i}} \right), \tag{31}$$

and

$$\dot{\varphi} + \Omega_e = O\left(\frac{v_{t,e}}{\rho_i}\sqrt{\frac{m_e}{m_i}}\right). \tag{32}$$

For functions $G = G(\bar{x}, U, \mu, \varphi)$, we define the operator $\mathcal{L}$ by

$$\mathcal{L}(G) = \dot{\bar{x}}\frac{\partial G}{\partial \bar{x}} + \dot{\mu}\frac{\partial G}{\partial \mu} + (\dot{\varphi} + \Omega_e)\frac{\partial G}{\partial \varphi}. \tag{33}$$

Equipped with this, the evolution equation for f_e becomes

$$\mathcal{L}(f_e) - \Omega_e\frac{\partial f_e}{\partial \varphi} = 0. \tag{34}$$

Using our scalings for the frequency of our new variables, we may find the scaling of $\mathcal{L}(G)$ to be

$$\mathcal{L}(G) = \underbrace{\dot{\bar{x}}\frac{\partial G}{\partial \bar{x}}}_{G\frac{v_{t,e}}{\rho_i}\alpha} + \underbrace{\dot{\mu}\frac{\partial G}{\partial \mu}}_{G\frac{v_{t,e}}{\rho_i}\sqrt{\frac{m_e}{m_i}}} + \underbrace{(\dot{\varphi} + \Omega_e)\frac{\partial G}{\partial \varphi}}_{G\frac{v_{t,e}}{\rho_i}\sqrt{\frac{m_e}{m_i}}}. \tag{35}$$

Our choice of variables has made the characteristic frequency of the operator $\mathcal{L}$ acting on G much smaller than the characteristic frequency of particle gyration. Note that presently the choice of ordering (11) or (13) does not change the overall scaling of $\mathcal{L}(G)$, which is dominated by the largest term, scaling with $\sqrt{m_e/m_i}$.

Now, for functions $G = G(\bar{x}, U, \mu, \varphi)$, we further define the gyroaverage of G, $\langle G \rangle_\varphi$, by

$$\langle G \rangle_\varphi = \frac{1}{2\pi}\int_0^{2\pi} G(\bar{x}, U, \mu, \varphi)\mathrm{d}\varphi. \tag{36}$$

This is an integral over the gyrophase at constant $\bar{x}$, μ and U. The gyroaverage allows us to decompose G into its gyrophase dependent and independent pieces,

$$G = \langle G \rangle_\varphi + \tilde{G}. \tag{37}$$

Decomposing f_e into its gyrophase dependent and independent pieces, we get

$$\mathcal{L}(\langle f_e \rangle_\varphi) + \mathcal{L}(\tilde{f}_e) - \Omega_e\frac{\partial \tilde{f}_e}{\partial \varphi} = 0. \tag{38}$$

We extract from this equation its gyrophase independent part

$$\langle \mathcal{L}(\langle f_e \rangle_\varphi) \rangle_\varphi + \langle \mathcal{L}(\tilde{f}_e) \rangle_\varphi = 0, \tag{39}$$

leaving the gyrophase dependent part

$$\Omega_e \frac{\partial \tilde{f}_e}{\partial \varphi} - \widetilde{\mathcal{L}(\tilde{f}_e)} = \widetilde{\mathcal{L}(\langle f_e \rangle_\varphi)}. \tag{40}$$

In order to solve equation (39) for the evolution of $\langle f_e \rangle_\varphi$, we need to know $\tilde{f}_e$. We can find $\tilde{f}_e$ by solving equation (40) perturbatively. We write $\tilde{f}_e = \tilde{f}_{e,1} + \tilde{f}_{e,2} + \dots$ and demand that $\tilde{f}_{e,1}$ solves

$$\Omega_e \frac{\partial \tilde{f}_{e,1}}{\partial \varphi} = \widetilde{\mathcal{L}(\langle f_e \rangle_\varphi)}, \tag{41}$$

and each subsequent term satisfies

$$\Omega_e \frac{\partial \tilde{f}_{e,n+1}}{\partial \varphi} = \widetilde{\mathcal{L}(\tilde{f}_{e,n})}. \tag{42}$$

By analysing the scalings of equations (41) and (42), and using equation (35), we find that $\tilde{f}_{e,1} \sim (m_e/m_i)\langle f_e \rangle_\varphi$. In Appendix A.1 we calculate the contribution of $\langle \mathcal{L}(\langle f_e \rangle_\varphi) \rangle_\varphi$ to equation (39). Using this we arrive at

$$- \alpha \langle v_\| \rangle_\varphi \frac{\partial \langle f_e \rangle_\varphi}{\partial \bar{x}} = O\left(\langle \mathcal{L}(\tilde{f}_{e,1}) \rangle_\varphi, \frac{v_{t,e}}{\rho_i} \frac{m_e}{m_i} \alpha \langle f_e \rangle_\varphi \right). \tag{43}$$

Neglecting the right hand side of equation (43),

$$- \alpha \langle v_\| \rangle_\varphi \frac{\partial \langle f_e \rangle_\varphi}{\partial \bar{x}} = 0. \tag{44}$$

This equation tells us that the gyroaveraged distribution function, written as a function of the total energy U and adiabatic invariant μ, is independent of $\bar{x}$. However, the left hand side of equation (44) scales with α. Therefore, for small α, we must carefully justify that the neglected terms of equation (43) are smaller than the term we retain. The second neglected term on the right hand side of equation (43) includes a factor of α, hence, is trivially smaller by a factor of mass ratio than the left hand side for all α. A naive glance at the other neglected term, $\langle \mathcal{L}(\tilde{f}_{e,1}) \rangle_\varphi$, would indicate that it has size $(m_e/m_i)^{3/2}$. Since this does not scale with α, this would imply that, in our small α ordering in equation (13), the errors in our equation for $\langle f_e \rangle_\varphi$ would have size $\sqrt{m_e/m_i}$. This is however, not the case, as we show in Appendix A.2 that the offending term which would appear to have size $(m_e/m_i)^{3/2}$ in fact cancels, leaving terms that are smaller in mass ratio in both orderings (11) and (13).

2.3. The ion model

With the electron model in section 2.2, we transformed to variables that were slowly varying over a single orbit. For the ions we will use the variables $\bar{x}$, $U_\perp$ and U defined by (17), (18) and (19), respectively. Analogously to the electrons, characteristics of the ion motion can be found that make the distribution function independent of $\bar{x}$ [14]. In contrast to the electrons, the radial extent of the ions is comparable to size of the presheath. Thus, the expansion in $x - \bar{x}$ that simplified the electron model is no longer valid for the ions. In order to determine the ion density at a given position x, we must ask what possible values of $\bar{x}$ and $U_\perp$ could give rise to particles in that position.

2.3.1. Closed orbits. Equation (23) defines the effective potential in which an ion with a given $\bar{x}$ and $U_\perp$ oscillates. We refer to an orbit as being closed if in the future it will have a bounce point, which is a point at which the x directed velocity of the particle changes sign. Since we have defined closed orbits in relation to bounce points, and bounce points are characterised by $\chi(x, \bar{x}) = U_\perp$, it is relevant to consider where the extrema of the effective potentials are. The locations of the extrema are given by the equation

$$\frac{\partial \chi}{\partial x}(x, \bar{x}) = \Omega_i^2(x - \bar{x}) + \frac{\Omega_i}{B}\phi'(x) = 0. \tag{45}$$

Thus,

$$\bar{x} - x = \frac{\phi'(x)}{\Omega_i B}. \tag{46}$$

Since we consider potentials with positive and monotonic decreasing derivative (see figure 1), we expect equation (46) to have zero, one or two solutions. This can be shown by defining the function $\xi(x)$,

$$\xi(x) = x + \frac{\phi'(x)}{\Omega_i B}. \tag{47}$$

Whenever $\xi(x) = \bar{x}$, the effective potential will have a stationary point. Furthermore, the effective potential will have positive gradient when $\xi(x) > \bar{x}$ and negative gradient when $\xi(x) < \bar{x}$. From figure 3, it is evident that, at low $\bar{x}$, there will be no solutions to equation (46) and the gradient of the effective potential will be positive for all x.

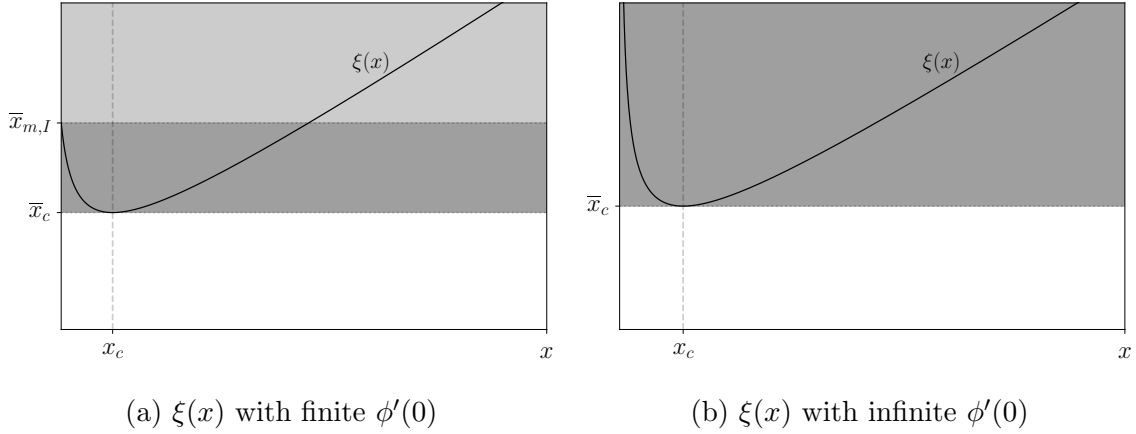(a) $\xi(x)$ with finite $\phi'(0)$ (b) $\xi(x)$ with infinite $\phi'(0)$

Figure 3: Curves $\xi(x)$, defined in equation (47), for two possible potentials in the presheath: one with finite gradient at $x = 0$, the other with infinite gradient. For a given value of $\bar{x}$, the effective potential $\chi(x, \bar{x})$ will have a stationary point wherever $\xi(x) = \bar{x}$. The effective potential will have negative gradient wherever $\bar{x} > \xi(x)$, and positive gradient wherever $\bar{x} < \xi(x)$. Thus, the effective potential gains a well for $\bar{x} > \bar{x}_c$. For $\bar{x}_{m,I} > \bar{x} > \bar{x}_c$ (shaded dark grey), the effective potential will then be a well with two extrema, creating a type 2 orbit. For $\bar{x} > \bar{x}_{m,I}$ (shaded light grey), the potential has only one extremum; a minimum, creating a type 1 orbit. Note that, in the right hand plot, the gradient of the potential is infinite at $x = 0$. Hence, there are always two solutions to equation (46) meaning all $\bar{x}$ give type 2 orbits. One possible $\xi(x)$ curve not shown is one where $\xi(x)$ is an increasing function of x, implying $x_c = 0$. Such a $\xi(x)$ would give rise to only type 1 orbits.

The first $\bar{x}$ for which equation (46) has a solution is $\bar{x}_c$, defined by

$$\bar{x}_c = \min_{x \in [0, \infty]} \left(x + \frac{\phi'(x)}{\Omega_i B} \right) = x_c + \frac{\phi'(x_c)}{\Omega_i B}. \tag{48}$$

For $\bar{x} > \bar{x}_c$ it is possible that equation (46) will have one or two solutions. Having two solutions implies the effective potential will have two stationary points (one maximum and one minimum), creating a potential well in which an ion could oscillate, provided its energy did not exceed that of the effective potential maximum. This is not the only type of potential well in which ion could oscillate, as all that is required for a potential well is a local minimum. Appealing once more to figure 3, we see that

equation (46) will only have one solution when $\bar{x}$ exceeds $\bar{x}_{m,I}$, defined by

$$\bar{x}_{m,I} = \frac{\phi'(0)}{\Omega_i B}. \tag{49}$$

The parameter region $\bar{x} > \bar{x}_{m,I}$ corresponds to the effective potential decreasing initially from $x = 0$ before reaching a minima and increasing. Thus, this also defines a simpler potential well in which the ion can oscillate.

We now introduce the nomenclature used in [14, 15, 23] to classify orbits. An orbit is referred to as being of 'type 1' if it has a single local minimum, and it is referred to as being of 'type 2' if it has a maxima and a minima. Effective potentials corresponding to these orbits are shown in figure 4 and we see from the above discussion that $\bar{x} > \bar{x}_{m,I}$ gives rise to type 1 orbits while $\bar{x}_{m,I} > \bar{x} > \bar{x}_c$ gives rise to type 2 orbits. Note that the derivative of the potential at $x = 0$ need not be finite and in such a case all orbits will be of type 2.

An ion associated with any of these effective potentials will be in a closed orbit provided the perpendicular energy, $U_\perp$, is not sufficient to allow the ion to reach the wall. In other words, the perpendicular energy must be less than the effective potential maximum, $\chi_M(\bar{x})$, defined by

$$\chi_M(\bar{x}) = \max_{x \in [0, x_c]} (\chi(x, \bar{x})) = \chi(x_M(\bar{x}), \bar{x}). \tag{50}$$

Here we have also defined $x_M(\bar{x})$, the x coordinate of the effective potential maximum for a given $\bar{x}$. Note that for type 1 orbits, $\chi_M(\bar{x}) = \chi(0, \bar{x})$ and $x_M(\bar{x}) = 0$.

In section 2.1, we showed that $\bar{x}$ slowly decreases in time. As such, for a given ion, $\chi_M(\bar{x})$ will also decrease slowly, eventually falling below $U_\perp$ (which is also decreasing, but more slowly). At this point, the ion will be free to travel towards $x = 0$ and is no longer considered to be on a closed orbit. To account for this effect, it is necessary not only to consider closed orbits, but also 'open orbits'

2.3.2. Open orbits. While closed orbits dominate throughout most of the presheath, in the area close to $x = 0$, there are much fewer closed orbits. Clearly we expect more orbits to become unbound as the ions drift slowly towards the wall. This motivates the fact that the presheath cannot be understood using only closed orbits and instead we need to include open orbits. We define an open orbit to be an ion trajectory which at a past time had bounce points and has no bounce points at
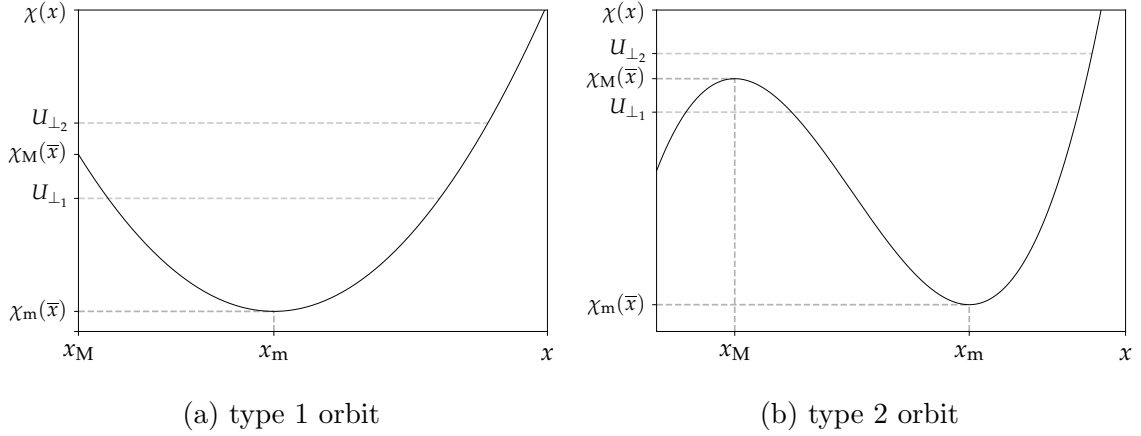
(a) type 1 orbit   (b) type 2 orbit

Figure 4: Examples of type 1 and type 2 orbits. Type 1 orbits have $x_M = 0$ and type 2 orbits have $x_M \geq 0$. Orbits with perpendicular energy $U_{\perp_1}$ will be closed orbits in both cases while orbits at $U_{\perp_2}$ will by open orbits. Note that the typical size of $U_{\perp_2}$ has been exaggerated for this sketch as open orbits will only have perpendicular energies marginally higher than $\chi_M(\bar{x})$.

future times. These orbits are of type 1 or type 2 depending on the type of closed orbit they last 'escaped' from. In reference [15], it was shown that the perpendicular energies of these open orbits was strongly concentrated around the effective potential maximum. This implies that the velocity distribution of the ions with a particular value of $\bar{x}$ near the wall is strongly concentrated around V_0, defined by

$$V_0 = -\sqrt{\chi_M(\bar{x}) - \chi(0, \bar{x})}. \tag{51}$$

Physically, this makes sense as the orbits in consideration are those that have only recently become unbound and therefore their perpendicular energy will be only a small amount above $\chi_M(\bar{x})$ because $U_\perp$ does not increase appreciably over a single orbit, by equation (21). Moreover, Geraldini et al [15] found that the velocity spread of ions in the x direction in open orbits is

$$\Delta v_x = \sqrt{2\left(\Delta_M + \chi_M(\bar{x}) - \chi(x, \bar{x})\right)} - \sqrt{2\left(\chi_M(\bar{x}) - \chi(x, \bar{x})\right)}, \tag{52}$$

where the function $\Delta_M(\bar{x}, U)$ is defined by

$$\Delta_M(\bar{x}, U) = 2\alpha\Omega_i^2 \sqrt{2(U - \chi_M(\bar{x}))} \int_{x_b}^{x_t} \frac{s - x_b}{\sqrt{2(\chi_M(\bar{x}) - \chi(s, \bar{x}))}} \mathrm{d}s, \tag{53}$$

and x_t and x_b are the top and bottom bounce points: the locations where the velocity in the x direction reverses in the quasiperiodic motion. Therefore $x_b = x_\mathrm{M}$ and x_t solves $\chi(x_t, \bar{x}) = \chi_\mathrm{M}(\bar{x})$ with $x_t > x_b$. Although Δ_M is, for most cases, not analytically tractable, its scaling will be sufficient for our purposes. We first examine the integral in equation (53). The denominator of the integral vanishes at both end points of the integral but it is otherwise finite. Dealing with the lower bounce point first, we see that the integrand is always finite since $\chi_\mathrm{M}(\bar{x}) - \chi(s, x)$ is at worst quadratic in $s - x_b$ as $s \to x_b$ (this occurs for type 2 orbits, see figure 4) and so the denominator $\sqrt{\chi_\mathrm{M}(\bar{x}) - \chi(s, x)}$ is at worst linear in $s - x_b$, which is cancelled by the numerator. At the upper bounce point, $\chi_\mathrm{M}(\bar{x}) - \chi(s, x)$ vanishes linearly as $s \to x_t$ for both type 1 and 2 orbits. Therefore, as the integrand contains an integrable singularity, the integral in equation (53) will scale as $v_\mathrm{t,i}/\Omega_\mathrm{i}^2$ regardless of the type of orbit, and we arrive at the overall scaling of $\Delta_M = O\left(\alpha v_\mathrm{t,i}^2\right)$. As a result of the size of Δ_M, when the ion is near the effective potential maximum, such that $\chi_\mathrm{M}(\bar{x}) - \chi(x, \bar{x}) \sim \Delta_\mathrm{M}$, $\Delta v_x = O\left(\sqrt{\alpha} v_\mathrm{t,i}\right)$ (by equation (52)). However, away from the effective potential maximum, we find $\Delta_\mathrm{M} \ll \chi_\mathrm{M}(\bar{x}) - \chi(x, \bar{x})$ giving $\Delta v_x = O\left(\alpha v_\mathrm{t,i}\right)$.

3. Ion and electron densities

To find the electron and ion densities, we calculate the following integral over the relevant distribution function,

$$n_\mathrm{s}(x) = \iiint f_\mathrm{s}(x, v_x, v_y, v_z) \mathrm{d}v_x \mathrm{d}v_y \mathrm{d}v_z. \tag{54}$$

Calculating this integral requires changing to coordinates in which the entrance distribution function is a constant. In these coordinates the dependence on x appears via the limits of integration. For ions, we will appeal to section 2.3 to find which orbits may still be present, while for the electrons we will discuss the 'cutoff potential' that accounts for electrons lost to the wall.

3.1. The ion density

The Jacobian of the transformation $\{v_x, v_y, v_z\} \rightarrow \{\bar{x}, U_\perp, U\}$ can be found from equations (17), (18) and (19) and is

$$\frac{\partial(v_x, v_y, v_z)}{\partial(\bar{x}, U_\perp, U)} = \frac{\Omega_i}{v_x v_z} = \Omega_i \frac{1}{\sqrt{2(U_\perp - \chi(x, \bar{x}))}} \frac{1}{\sqrt{2(U - U_\perp)}}. \tag{55}$$

In line with [15], we denote the closed orbit ion distribution function as a function of the conserved variables $\{\mu, U\}$ to be $F_{cl}(\mu, U)$. Here, the adiabatic invariant for ions plays an analogous role to the adiabatic invariant for electrons and is defined in [15] as a function of the variables $\bar{x}$ and $U_\perp$. Hence the density integral (54) is transformed to

$$n_i(x) = \sum_{\sigma_\parallel = \pm 1} \int \Omega_i d\bar{x} \int \frac{2 dU_\perp}{\sqrt{2(U_\perp - \chi(x, \bar{x}))}} \int \frac{F_{cl}(\mu(\bar{x}, U_\perp), U, \sigma_\parallel)}{\sqrt{2(U - U_\perp)}} dU. \tag{56}$$

The sum is over the particles with positive and negative z directed velocities. A similar sum exists over the positive and negative x directed velocities but, since the distribution function is gyrophase independent at lowest order, this simply becomes a factor of 2. All that remains is to find the appropriate limits on the coordinates to ensure that only true closed orbits are being integrated over. Consider an ion at position x. For this ion to be in a closed orbit, two conditions must be met: first, there must be a point in the ions effective potential at $s < x$ such that $\chi(s, \bar{x}) > \chi(x, \bar{x})$. This implies

$$\frac{1}{2}\Omega_i^2(x - \bar{x})^2 + \frac{\Omega_i \phi(x)}{B} < \frac{1}{2}\Omega_i^2(s - \bar{x})^2 + \frac{\Omega_i \phi(s)}{B}, \tag{57}$$

which rearranges to give

$$\bar{x} > \frac{1}{2}(x + s) + \frac{\phi(x) - \phi(s)}{\Omega_i B(x - s)}. \tag{58}$$

The minimum possible value of $\bar{x}$ for which this condition could be satisfied is $\bar{x}_m(x)$, defined by

$$\bar{x}_m(x) = \min_{s \in [0,x)} \left(\frac{1}{2}(x + s) + \frac{\phi(x) - \phi(s)}{\Omega_i B(x - s)} \right), \tag{59}$$

giving the condition $\bar{x} > \bar{x}_m(x)$. Having chosen a possible $\bar{x}$, the second condition for a closed orbit is that the particle must not have sufficient perpendicular energy

to pass the maximum of the effective potential. This amounts to an upper bound on $U_\perp$ of $\chi_M(\bar{x})$. The only condition on the parallel energy is that the velocity in the z direction must be real valued. The resulting ion density integral is given by

$$n_{\text{i,cl}}(x) = \int_{\bar{x}_m(x)}^{\infty} \Omega_s d\bar{x} \int_{\chi(x,\bar{x})}^{\chi_M(\bar{x})} \frac{2dU_\perp}{\sqrt{2\left(U_\perp - \chi(x,\bar{x})\right)}} \int_{U_\perp}^{\infty} \frac{F_{\text{cl}}(\mu(\bar{x}, U_\perp), U)}{\sqrt{2\left(U - U_\perp\right)}} dU. \quad (60)$$

Here we have also removed the sum over parallel directions due to that fact that no ions are reflected back from the sheath into the presheath.

As well as closed orbits, we must also consider open orbits. Just as with closed orbits, we make the same change of variables from $\{v_x, v_y, v_z\}$ to $\{\bar{x}, U_\perp, U\}$. However, we must impose different limits on the allowed values of these coordinates at a given x. To do so, we note that an ion on an open orbit will hit the wall on a timescale of order $1/\Omega_i$. Thus we may exploit the smallness of equations (20) and (21) to argue that the value of $\bar{x}$ and $U_\perp$ that this ion had a time of order $1/\Omega_i$ before will not change appreciably. An orbit becomes open when $U_\perp$ grows minutely larger than the value of the effective potential maximum $\chi_M(\bar{x})$ that had stopped the ion from reaching the wall. This small increase will however leave the upper bounce point x_t virtually unchanged. This means that, as an ion transitions into an open orbit, it can be found anywhere between $x = 0$ and the upper bounce point of the closed orbit it previously occupied. Therefore, ions in open orbits at positions $x > x_c$ cannot have come from orbits with $\bar{x} < \bar{x}_m(x)$ for the same reason closed orbits at this position could not come from this $\bar{x}$: the perpendicular energy required to reach x from that $\bar{x}$ would imply the orbit had been open for much longer than one period of the motion and thus no ions could exist on such an orbit. If $x < x_c$, however, all open orbits are free to move towards $x = 0$ (by definition) and hence an ion with $x < x_c$ could have come from any valid closed orbit: $\bar{x} > \bar{x}_c$. We denote the minimum $\bar{x}$ for an open orbit at position x to be $\bar{x}_{\text{m,o}}$ given by

$$\bar{x}_{\text{m,o}} = \begin{cases} \bar{x}_c \text{ if } x \leq x_c, \\ \bar{x}_m(x) \text{ if } x > x_c. \end{cases} \quad (61)$$

Once we have established the value of $\bar{x}$ that an ion in an open orbit previously had, we can determine the range of possible v_x. As argued above, it is only a minute change in $U_\perp$ that causes an orbit to become open so v_x will be tightly concentrated

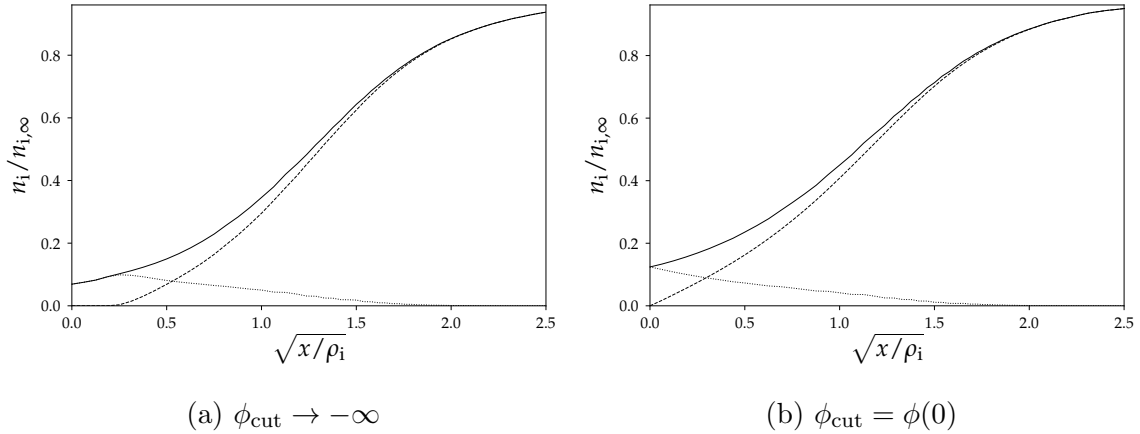(a) $\phi_{\rm cut} \to -\infty$ (b) $\phi_{\rm cut} = \phi(0)$

Figure 5: Ion density (solid line) composed of closed (dashed) and open (dotted) orbit densities for two solutions with different cutoff potentials. For these simulations, $\alpha = 0.05$, and we use the boundary conditions specified in section 6 with $T_{\rm e} = T_{\rm i}$

around a single value. This is made precise by (52). Thus,

$$
n_{\rm i,op}(x) = \int_{\bar{x}_{\rm m,o}}^{\infty} \Omega_{\rm i} {\rm d}\bar{x} \int_{\chi_{\rm M}(\bar{x})}^{\infty} \frac{F_{\rm cl}(\mu(\bar{x}, \chi_{\rm M}(\bar{x})), U)}{\sqrt{2\left(U - \chi_{\rm M}(\bar{x})\right)}} \Delta v_x \, {\rm d}U. \tag{62}
$$

While the presence of Δv_x ensures that the open orbit density is everywhere small, it is still the dominant contribution to the ion density near $x = 0$, where the closed orbit ion density tends to zero. We can see from figure 5 that this is indeed true and that in all cases it would be a mistake to neglect the contribution of the open orbits to the ion density.

As discussed in the introduction, the scaling of $n_{\rm i,op}(x)$ with α near $x = 0$ is of special importance due to its relation to the total potential drop in the presheath. By definition, type 1 orbits have their effective potential maximum at $x = 0$, while the locations of the maxima of type 2 effective potentials occupy a continuous range of x. Recalling the discussion at the end of section 2.3, we see that, away from $x = 0$, the vast majority of ions are not near their effective potential maximum, and so $\Delta v_x = O\left(\alpha v_{\rm t,i}\right)$ which therefore implies $n_{\rm i,op}(x) = O(\alpha n_{\rm i,\infty})$. As we approach $x = 0$, however, if there is a significant number of type 1 orbits present, these orbits will be near their effective potential maxima, and as such will have $\Delta v_x = O(\sqrt{\alpha} v_{\rm t,i})$. This means that if type 1 orbits are present, $n_{\rm i,op}(0) = n_{\rm i}(0) = O(\sqrt{\alpha} n_{\rm i,\infty})$. On the

other hand, if only type 2 orbits are present, $n_i(0) = O(\alpha n_{i,\infty})$. This is the algebraic counterpart to the argument based on circular orbits in figure 2 as orbits that are not significantly deformed by the potential are naturally of type 1.

By conservation of particle flux, we know that the product of the ion density and fluid velocity is constant. Therefore, when only type 2 orbits are present, the fluid velocity towards the wall is much larger than when type 1 and type 2 orbits are present. In section 4.2 we will see that this is an early sign of how the Bohm condition will emerge from the theory, and how the presence of type 1 orbits can have a startling impact on the presheath.

3.2. The electron density

The electron density at any position x is given by

$$n_e(x) = \iiint f_e(x, v_x, v_y, v_z) \mathrm{d}v_x \mathrm{d}v_y \mathrm{d}v_z, \tag{63}$$

over suitable limits. The Jacobian for the coordinate transformation to $\{U, \mu, \varphi\}$ is given by

$$\left| \frac{\partial(v_x, v_y, v_z)}{\partial(U, \mu, \varphi)} \right| = \frac{\Omega_e}{|v_\parallel|}. \tag{64}$$

So we have

$$n_e(x) = \sum_{\sigma_\parallel = \pm 1} \int \mathrm{d}\varphi \int \Omega_e \mathrm{d}\mu \int \frac{\langle f_e \rangle_\varphi}{|v_\parallel|} \mathrm{d}U + O\left(\frac{m_e}{m_i} n_e \right), \tag{65}$$

where the sum is over electrons moving into ($\sigma_\parallel = 1$) and out of ($\sigma_\parallel = -1$) the presheath. Here, we have exploited the decomposition of f_e in equation (37) into its gyrophase dependent and independent pieces. From this we may exploit the independence of $\langle f_e \rangle_\varphi$ on $\bar{x}$ to use the gryoaveraged distribution function evaluated at infinity. All that remains is to calculate the appropriate limits on the gyrophase, adiabatic invariant and energy.

The effect of the potential drop within the presheath is to decelerate electrons in the direction parallel to the magnetic field. In Appendix A.1 we write the total energy U as

$$U = \Omega_e \mu - \frac{\Omega_e}{B} \phi(x) + \frac{1}{2} v_\parallel^2 + v_y v_E + O\left(v_{t,e}^2 \frac{m_e}{m_i} \right). \tag{66}$$

Since the total energy and the adiabatic invariant are constant within the presheath, the parallel velocity must decrease to compensate for the potential drop (the $\mathbf{E} \times \mathbf{B}$ drift will not compensate for the potential drop as it is smaller than the electron thermal speed by a factor of $\sqrt{m_e/m_i}$). Thus, an electron that enters the presheath at a finite velocity may at some point be reflected. As such, the minimum value of the total energy for a particle at position x with adiabatic invariant μ and gyrophase φ corresponds to a particle that has zero parallel velocity. Thus,

$$U_{\min} = \Omega_e \mu - \frac{\Omega_e}{B}\phi(x) + v_y v_E + O\left(v_{t,e}^2 \frac{m_e}{m_i}\right). \tag{67}$$

Note that the term $v_y v_E$ in equation (67) makes $U_{\min}$ a function of $\bar{x}$ as well as x. However, this correction is small (of size $\sqrt{m_e/m_i}$), and will gyroaverage to be of size m_e/m_i, so will turn out to be unimportant. The maximum possible parallel velocity for an electron entering the presheath is infinite since particles can enter the presheath at any speed. Hence, the maximum energy for an electron entering the presheath is also infinite. For electrons exiting the presheath, however, a different consideration must be made. We assume that an electron that reaches the wall of the device is absorbed onto the wall and does not return to the presheath. Then, if an electron is leaving the presheath (i.e. has negative parallel velocity), it must have been reflected before reaching the wall. Therefore, there must be a maximum energy of these particles leaving the presheath that depends on the adiabatic invariant, which we denote by $U_{\max}(\mu)$. To determine the value of $U_{\max}(\mu)$, we must consider which particles are lost to the wall within the Debye sheath. Energy is conserved for particles entering the Debye sheath. If we further assume that the adiabatic invariant of an electron is the same as it was when that electron entered the Debye sheath, we may parametrise $U_{\max}$ by the function $\Phi(\mu, \Delta\phi_{DS})$ (where we have denoted the potential drop in the Debye sheath, $\phi(0) - \phi_{cut}$, by $\Delta\phi_{DS}$), declaring

$$U_{\max}(\mu) = \Omega_e \mu - \frac{\Omega_e}{B}\phi_{cut} - \frac{\Omega_e}{B}\Phi(\mu, \Delta\phi_{DS}), \tag{68}$$

where the choice to isolate the $\Omega_e \mu$ is arbitrary, but driven by the form of our expressions for U, which in Appendix A.1 we write as

$$U = \Omega_e \mu + \frac{v_\parallel^2}{2} - \frac{\Omega_e}{B}\phi(\bar{x}), \tag{69}$$

with errors small by mass ratio. In general the physics of absorption onto the wall of a plasma is complicated by the fact that the length scale of the Debye sheath, which is a few Debye lengths λ_{D}, is of the order of the electron gyroradius, leading to a complex form of $\Phi(\mu, \Delta\phi_{\mathrm{DS}})$, depending implicitly on the form of the electron and ion distribution functions at the Debye sheath entrance as well as on μ and $\Delta\phi_{\mathrm{DS}}$.

Inserting the relevant limits on our variables, we arrive at the following expression for the electron density at position x

$$
n_{\mathrm{e}}(x) = \int_0^{2\pi} \mathrm{d}\varphi \int_0^\infty \Omega_{\mathrm{e}}\mathrm{d}\mu \left[\int_{\Omega_{\mathrm{e}}\mu - \frac{\Omega_{\mathrm{e}}}{B}\phi(x)+v_y v_E}^\infty \frac{\langle f_e\rangle_\varphi(U,\mu)\mathrm{d}U}{\sqrt{2\left(U - \Omega_{\mathrm{e}}\mu + \frac{\Omega_{\mathrm{e}}}{B}\phi(x) - v_y v_E\right)}} \right.
$$
$$
\left. + \int_{\Omega_{\mathrm{e}}\mu - \frac{\Omega_{\mathrm{e}}}{B}\phi(x)+v_y v_E}^{\Omega_{\mathrm{e}}\mu - \frac{\Omega_{\mathrm{e}}}{B}\phi_{\mathrm{cut}} - \frac{\Omega_{\mathrm{e}}}{B}\Phi(\mu,\Delta\phi_{\mathrm{DS}})} \frac{\langle f_e\rangle_\varphi(U,\mu)\mathrm{d}U}{\sqrt{2\left(U - \Omega_{\mathrm{e}}\mu + \frac{\Omega_{\mathrm{e}}}{B}\phi(x) - v_y v_E\right)}} \right]. \tag{70}
$$

Here, the integral over U has been explicitly split into the incoming and outgoing particles, contained in the first and second terms, respectively. The factors of $v_y v_E$ in equation (70) are due to the fact that we aim to evaluate the potential at a given position x rather than at $\bar{x}$. However, these factors are small by $\sqrt{m_{\mathrm{e}}/m_{\mathrm{i}}}$ and the integral can be Taylor expanded in them. After expanding, it is a simple task to show that the lowest order correction due to $v_y v_E$ vanishes when integrating over φ leaving a correction of size $m_{\mathrm{e}}/m_{\mathrm{i}}$, which we neglect. We therefore arrive at an expression for the electron density that depends only on the input distribution function, the local potential, and the cutoff potential

$$
n_{\mathrm{e}}(x) = 2\pi \int_0^\infty \Omega_{\mathrm{e}}\mathrm{d}\mu \left[\int_{\Omega_{\mathrm{e}}\mu - \frac{\Omega_{\mathrm{e}}}{B}\phi(x)}^\infty \frac{\langle f_e\rangle_\varphi(U,\mu)\mathrm{d}U}{\sqrt{2\left(U - \Omega_{\mathrm{e}}\mu + \frac{\Omega_{\mathrm{e}}}{B}\phi(x)\right)}} \right.
$$
$$
\left. + \int_{\Omega_{\mathrm{e}}\mu - \frac{\Omega_{\mathrm{e}}}{B}\phi(x)}^{\Omega_{\mathrm{e}}\mu - \frac{\Omega_{\mathrm{e}}}{B}\phi_{\mathrm{cut}} - \frac{\Omega_{\mathrm{e}}}{B}\Phi(\mu,\Delta\phi_{\mathrm{DS}})} \frac{\langle f_e\rangle_\varphi(U,\mu)\mathrm{d}U}{\sqrt{2\left(U - \Omega_{\mathrm{e}}\mu + \frac{\Omega_{\mathrm{e}}}{B}\phi(x)\right)}} \right]. \tag{71}
$$

Important features of this density can be seen easily by making the change of variables from U to $\bar{v}_\parallel$ defined by

$$
\bar{v}_\parallel = \sqrt{2\left(U - \Omega_{\mathrm{e}}\mu + \frac{\Omega_{\mathrm{e}}}{B}\phi(x)\right)}. \tag{72}
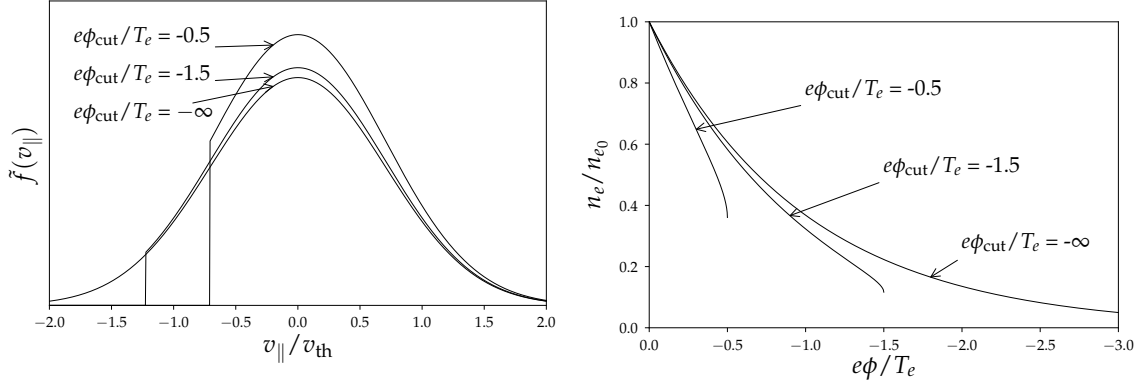$$

(a) Example marginalised electron distribution function in $v_\parallel$

(b) Electron density as a function of ϕ

Figure 6: Here we see an example entrance distribution (the truncated Maxwellian) that has a discontinuity. The effect of this discontinuity is to create a square root like dependence as ϕ approaches $\phi_{\rm cut}$. Note that as the $\phi_{\rm cut}$ is taken to infinity the distribution tends to a Maxwellian and the density profile to a Boltzmann distribution, as equation (71) would imply.

This changes equation (71) to

$$
\begin{aligned}
n_{\rm e}(x) = 2\pi \int_0^\infty \Omega_{\rm e}{\rm d}\mu &\left[\int_0^\infty \langle f_e \rangle_\varphi \left(\Omega_{\rm e}\mu + \frac{\bar{v}_\parallel^2}{2} - \frac{\Omega_{\rm e}}{B}\phi(x), \mu \right) {\rm d}\bar{v}_\parallel \right. \\
&\left. + \int_0^{\sqrt{2\frac{\Omega_{\rm e}}{B}(\phi(x)-\phi_{\rm cut}-\Phi(\mu,\Delta\phi_{\rm DS}))}} \langle f_e \rangle_\varphi \left(\Omega_{\rm e}\mu + \frac{\bar{v}_\parallel^2}{2} - \frac{\Omega_{\rm e}}{B}\phi(x), \mu \right) {\rm d}\bar{v}_\parallel \right].
\end{aligned}
\tag{73}
$$

In the limit $\rho_{\rm e}/\lambda_{\rm D} \ll 1$, we expect that the electron orbit width can be neglected. Neglecting the electron orbit width is equivalent to assuming that the electrons are absorbed when they reach a value of $\bar{x}$ corresponding to the wall, such that $\phi(\bar{x}) = \phi_{\rm cut}$. Appealing to equations (68) and (69), this corresponds to the assumption of $\Phi(\mu, \Delta\phi_{\rm DS}) = 0$. This justifies our convention on $\Phi(\mu, \Delta\phi_{\rm DS})$ in equation (68) as it isolates the potential required to reach the wall in this limit. Another case where we expect this to apply is when the potential drop in the Debye sheath is small, so that the complex influence of the sheath is virtually not present.

This is the limit of $\phi(0) - \phi_{\text{cut}}$ becoming small, thus,

$$\lim_{\Delta\phi_{\text{DS}}\to 0} \Phi(\mu, \Delta\phi_{\text{DS}}) = 0. \tag{74}$$

It therefore follows that the derivative of the electron density with respect to potential at $x = 0$ will diverge as $\phi(0) \to \phi_{\text{cut}}$. This can be seen in figure 6, where we plot n_{e} as a function of ϕ for the particular case of $\Phi(\mu, \Delta\phi_{\text{DS}}) = 0$ with a truncated Maxwellian input electron distribution function. In section 4 we will prove the infinite derivative in n_{e} at $x = 0$ to be an important distinction from the Maxwell-Boltzmann response. Since this feature will be present for a general model, for the remainder of this paper we shall specialise to the simplest model, $\Phi(\mu, \Delta\phi_{\text{DS}}) = 0$.

4. Quasineutrality

The solutions to the collisionless magnetic presheath are expected to be quasineutral and thus satisfy the equation

$$n_{\text{e}}(x) = Zn_{\text{i}}(x). \tag{75}$$

The problem of solving the magnetic presheath amounts to finding a potential throughout the presheath such that equation (75) is satisfied. Building on the expansions in [15] of the quasineutrality equation, we investigate the behaviour of the quasineutrality equation for large and small x in sections 4.1 and 4.2, respectively. In the expansion at $x \to \infty$, we will recover the 'kinetic Chodura condition' from [15], but with a small alteration due to the truncated distribution for the electrons. Similarly, in section 4.2.1 we alter the 'kinetic Bohm condition' result of [15] which we will further show in section 4.2.2 to be broken for $\phi_{\text{cut}} = \phi(0)$.

4.1. Expansion at $x \to \infty$

Following the path paved in [15], we take the limit $x \to \infty$ under the assumptions

$$|\hat{\phi}| = \frac{e|\phi|}{T_{\text{e}}} \ll 1, \tag{76}$$

$$\epsilon = \frac{\rho_{\text{i}}\phi'}{\phi} \ll 1. \tag{77}$$

As discussed in [15], this is not the most general limit possible but suffices given our choice of entrance distribution functions, which will be detailed in section 6.2. Under

assumptions (76) and (77), it was shown that the expansion of the ion density at $x \to \infty$ was given by

$$n_{i,cl}(x) = \left(1 + \frac{\phi''(x)}{\Omega_i B}\right) \int_{-\pi}^{\pi} d\varphi \int_0^{\infty} \Omega_i d\mu \left\{ \int_{\Omega_i \mu}^{\infty} \frac{F_{cl}(\mu, U)}{\sqrt{2(U - \Omega_i \mu)}} dU - \sqrt{2\delta U_{\perp}} F_{cl}(\mu, \Omega_i \mu) \right.$$

$$- \delta U_{\perp} \int_{\Omega_i \mu}^{\infty} \frac{\partial F_{cl}(\mu, U)}{\partial U} \frac{dU}{\sqrt{2(U - \Omega_i \mu)}} + \frac{1}{3} (2\delta U_{\perp})^{\frac{3}{2}} \frac{\partial F_{cl}}{\partial U}(\mu, \Omega_i \mu)$$

$$\left. + \frac{1}{2} \delta U_{\perp}^2 \int_{\Omega_i \mu}^{\infty} \frac{\partial^2 F_{cl}(\mu, U)}{\partial U^2} \frac{dU}{\sqrt{2(U - \Omega_i \mu)}} \right\} + O(\hat{\phi} \epsilon n_{e,\infty}, \hat{\phi}^2 \epsilon^2 n_{e,\infty}, \hat{\phi}^{\frac{5}{2}} n_{e,\infty}),$$

$$(78)$$

where

$$\delta U_{\perp} = -\frac{\Omega_i \phi(x)}{B} + \frac{\Omega_i \phi'(x)}{B} \sqrt{\frac{2\mu}{\Omega_i}} \cos \varphi - \frac{\mu \phi''(x)}{2B} \left(1 + 2\cos^2 \varphi\right) + O(\hat{\phi} \epsilon n_{e,\infty}, \hat{\phi}^2 \epsilon^2 n_{e,\infty}). \tag{79}$$

Here, going to $x \to \infty$ has allowed the transformation of variables from $\bar{x}$ to the gyrophase φ for the ions. This is because the gradients of the field have decreased sufficiently to allow for an approximation of the orbits as circular, analogously to the electrons. Since we have changed only the way we describe the electrons in the presheath, this expression is identical to that in [15]. However, we must change the expansion of $n_e(x)$ at $x \to \infty$. By Taylor expanding the electron density as a function of $\hat{\phi} = e\phi/T_e$ (the dimensionless potential), we get

$$n_e(\phi) = n_{e,\infty} + \frac{dn_e}{d\hat{\phi}} \hat{\phi} + \frac{d^2 n_e}{d\hat{\phi}^2} \hat{\phi}^2 + O(\hat{\phi}^3 n_{e,\infty}), \tag{80}$$

where all derivatives are evaluated at $\phi = 0$. Note that, in the case of infinite cutoff potential and Maxwellian input, the derivatives are simply $n_{e,\infty}$ as the electrons are Boltzmann distributed (see figure 6). As in [15], collecting the zeroth order terms gives us the quasineutrality condition at $x \to \infty$,

$$n_{e,\infty} = Z \int_{-\pi}^{\pi} d\varphi \int_0^{\infty} \Omega_i d\mu \int_{\Omega_i \mu}^{\infty} \frac{F_{cl}(\mu, U)}{\sqrt{2(U - \Omega_i \mu)}}. \tag{81}$$

Gathering the terms that are proportional to $\hat{\phi}^{\frac{1}{2}}$, we (unsurprisingly) recover another identical result from [15]

$$Z \int_{-\pi}^{\pi} d\varphi \int_0^{\infty} \Omega_i d\mu \sqrt{2\delta U_{\perp}} F_{cl}(\mu, \Omega_i \mu) = 0, \tag{82}$$

which since F_{cl} is everywhere non-negative implies that $F_{\mathrm{cl}}(\mu, \Omega_{\mathrm{i}}\mu) = 0$. This is an expected result for a negatively charged wall from which no ions should return. The first deviation from the expansion in [15] occurs at first order in ϕ. We collect all terms linear in ϕ or one of its derivatives. Note the first derivative of ϕ will not be present due to the $\cos\varphi$ terms integrating to zero. The only terms left are proportional to ϕ and ϕ'',

$$\phi''(x) = k_1\phi(x) + O(\hat{\phi}\epsilon^3). \tag{83}$$

Here we have defined an analogous parameter, k_1, to that found in [15],

$$k_1 = \frac{\Omega_{\mathrm{i}}^2 m_{\mathrm{i}}}{ZT_{\mathrm{e}}} \frac{\frac{\mathrm{d}n_{\mathrm{e}}}{\mathrm{d}\hat{\phi}} - 2\pi \frac{Z^2 T_{\mathrm{e}}}{m_{\mathrm{i}}} \int_0^\infty \Omega_{\mathrm{i}}\mathrm{d}\mu \int_{\Omega_{\mathrm{i}}\mu}^\infty \frac{F_{\mathrm{cl}}(\mu,U)\mathrm{d}U}{(2(U-\Omega_{\mathrm{i}}\mu))^{\frac{3}{2}}}}{n_{\mathrm{e},\infty} + 2\pi Z \int_0^\infty \Omega_{\mathrm{i}}^2 \mu\mathrm{d}\mu \int_{\Omega_{\mathrm{i}}\mu}^\infty \frac{F_{\mathrm{cl}}(\mu,U)\mathrm{d}U}{(2(U-\Omega_{\mathrm{i}}\mu))^{\frac{3}{2}}}}. \tag{84}$$

This equation is solved by $\phi(x) \propto \exp(-\sqrt{k_1}x)$ and thus for a decaying solution at $x \to \infty$, we require $k_1 \geq 0$. This is a condition on ϕ_{cut} and the entrance ion distribution function for there to be a solution to these equations,

$$2\pi Z v_B^2 \int_0^\infty \Omega_{\mathrm{i}}\mathrm{d}\mu \int_{\Omega_{\mathrm{i}}\mu}^\infty \frac{F_{\mathrm{cl}}(\mu,U)\mathrm{d}U}{\left(2(U-\Omega_{\mathrm{i}}\mu)\right)^{\frac{3}{2}}} \leq \frac{\mathrm{d}n_{\mathrm{e}}}{\mathrm{d}\hat{\phi}}. \tag{85}$$

Equation (85) can further be expressed as

$$Z \iiint \frac{f_{\mathrm{i},\infty}(\mathbf{v})}{v_z^2}\mathrm{d}v_x\mathrm{d}v_y\mathrm{d}v_z \leq \frac{1}{v_B^2}\frac{\mathrm{d}n_{\mathrm{e}}}{\mathrm{d}\hat{\phi}}. \tag{86}$$

This is generalisation of the '*kinetic Chodura condition*' given in [15] to a presheath with a general electron distribution function. It is likely that just as the magnetic presheath will, in most cases, satisfy the kinetic Bohm condition with equality, a full treatment of the plasma outside the magnetic presheath would result in distribution functions marginally satisfying the modified kinetic Chodura condition [1].

4.2. Expansion around $x \to 0$

While at infinity we were safe to assume that the potential had a Taylor expansion in x, care must be taken as we approach the Debye sheath entrance. Indeed, it was shown in [15] that an infinite gradient at the origin would always be present within their formalism.

With this in mind, in this section we will first expand quasineutrality in the parameter $\delta\phi$ defined by

$$\delta\phi = \phi(x) - \phi(0). \tag{87}$$

Thus we will not make any assumptions about the nature of $\delta\phi$ save for the fact that it is finite (equivalent to the statement that the potential is finite at the origin). We conduct this expansion for two cases: first, in the usual case of $\phi(0) \neq \phi_{\mathrm{cut}}$, and secondly, in the special case of $\phi(0) = \phi_{\mathrm{cut}}$.

4.2.1. $\phi(0) \neq \phi_{\mathrm{cut}}$. From equation (73), we see that the electron density will have a Taylor expansion in $\delta\phi$, giving

$$n_{\mathrm{e}}(\phi) - n_{\mathrm{e}}(\phi(0)) = \frac{\mathrm{d}n_{\mathrm{e}}}{\mathrm{d}\phi}\delta\phi + \frac{1}{2}\frac{\mathrm{d}^2 n_{\mathrm{e}}}{\mathrm{d}\phi^2}\delta\phi^2 + O\left(n_{\mathrm{e}}(0)\left(\frac{\mathrm{e}}{T_{\mathrm{e}}}\delta\phi\right)^3\right). \tag{88}$$

The ion density at the origin has contributions from both open and closed orbits. In [15], it was shown that the leading order term of $n_{\mathrm{i,cl}}$ is due to closed type 1 orbits and gives a contribution of

$$n_{\mathrm{i,cl,I}}(x) = 2\int_{\bar{x}_{\mathrm{m,I}}}^{\infty} \sqrt{2\delta\chi}\,\Omega_{\mathrm{i}}\mathrm{d}\bar{x} \int_{\chi_{\mathrm{M}}(\bar{x})}^{\infty} \frac{F_{\mathrm{cl}}(\mu(\bar{x},\chi_{\mathrm{M}}(\bar{x})),U)}{\sqrt{2\left(U - \chi_{\mathrm{M}}(\bar{x})\right)}}\mathrm{d}U, \tag{89}$$

where $\delta\chi$ is defined as

$$\delta\chi = \chi(0,\bar{x}) - \chi(x,\bar{x}) = \Omega_{\mathrm{i}}^2 x\bar{x} - \frac{\Omega_{\mathrm{i}}}{B}\delta\phi + O\left(\left(\frac{x}{\rho_{\mathrm{i}}}\right)^2 v_{\mathrm{t,i}}^2\right). \tag{90}$$

Thus, all that remains to consider is the contribution from open orbits. To this end, we rewrite equation (62) as

$$\begin{aligned}
n_{\mathrm{i,op}}(x) - n_{\mathrm{i,op}}(0) &= \int_{\bar{x}_{\mathrm{c}}}^{\infty} \Omega_{\mathrm{i}}\mathrm{d}\bar{x} \int_{\chi_{\mathrm{M}}(\bar{x})}^{\infty} \frac{F_{\mathrm{cl}}(\mu,U)}{\sqrt{2\left(U - \chi_{\mathrm{M}}(\bar{x})\right)}}\left[\Delta v_x - \Delta v_{x_0}\right]\mathrm{d}U \\
&\quad - \int_{\bar{x}_{\mathrm{c}}}^{\bar{x}_{\mathrm{m,o}}} \Omega_{\mathrm{i}}\mathrm{d}\bar{x} \int_{\chi_{\mathrm{M}}(\bar{x})}^{\infty} \frac{F_{\mathrm{cl}}(\mu,U)}{\sqrt{2\left(U - \chi_{\mathrm{M}}(\bar{x})\right)}}\Delta v_x\mathrm{d}U,
\end{aligned} \tag{91}$$

where we have defined Δv_{x_0} as

$$\Delta v_{x_0} = \sqrt{2\left(\Delta_{\mathrm{M}} + \chi_{\mathrm{M}}(\bar{x}) - \chi(0,\bar{x})\right)} - \sqrt{2\left(\chi_{\mathrm{M}}(\bar{x}) - \chi(0,\bar{x})\right)}. \tag{92}$$

If type 2 orbits are present, then $x_c > 0$. Hence, sufficiently close to $x = 0$, we will have $x < x_c$ and the second integral in equation (91) will be zero by equation (61). If no type 2 orbits are present, then the second integral scales like $\bar{x}_m(x)$, defined in equation (59), which in turn scales like x or $\delta\phi$ and is small compared to $\sqrt{\delta\phi}$. Hence, only the first term in equation 91 can give a contribution comparable to that of $n_{i,cl}$. The size of the first term in equation (91) is set by $\Delta v_x - \Delta v_{x_0}$ which is given by

$$\Delta v_x - \Delta v_{x_0} = \sqrt{2\left(\Delta_M + \chi_M(\bar{x}) - \chi(x,\bar{x})\right)} - \sqrt{2\left(\chi_M(\bar{x}) - \chi(x,\bar{x})\right)} \tag{93}$$
$$- \sqrt{2\left(\Delta_M + \chi_M(\bar{x}) - \chi(0,\bar{x})\right)} + \sqrt{2\left(\chi_M(\bar{x}) - \chi(0,\bar{x})\right)}.$$

Depending on $\bar{x}$, $\Delta v_x - \Delta v_{x_0}$ will be evaluated for a type 1 orbit or a type 2 orbit. For a type 1 orbit, $\chi_M(\bar{x}) = \chi(0,\bar{x})$ so the last term in equation (93) is zero and the first and third terms differ by a term of order $\delta\chi$, while the second term, of order $\delta\chi^{1/2}$, would be the largest. If instead we are on a type 2 orbit, since $\chi_M(\bar{x}) \geq \chi(0,\bar{x})$, we may choose x sufficiently small that the above terms cancel leaving a piece of size at most $\delta\chi$ (first term cancels with third, second cancels with fourth). As such, to lowest order, we need only consider the part of the integral for which we are on a type 1 orbit, corresponding to a lower limit on $\bar{x}$ of $\bar{x}_{m,I}$.

After this, the lowest order term in the quasineutrality equation is

$$0 = \int_{\bar{x}_{m,I}}^\infty \sqrt{2\delta\chi}\,\Omega_i \mathrm{d}\bar{x} \int_{\chi_M(\bar{x})}^\infty \frac{F_{cl}(\mu, U)}{\sqrt{2\left(U - \chi_M(\bar{x})\right)}}\mathrm{d}U. \tag{94}$$

Given that the integrand is always positive, this equation is only satisfied if $\bar{x}_{m,I} \to \infty$, which by equation (49) implies the gradient of the potential is divergent at the origin.

This divergence offers a considerable simplification to the quasineutrality equation: with an infinite gradient at the origin, all effective potentials are of type 2 and so all ion trajectories will be open a finite distance before $x = 0$. By examining equation (59), we see that $\bar{x}_m(x)$ (the minimum allowed $\bar{x}$ for a closed orbit to be present) diverges at small x (as we now expect). From this, we see that $\bar{x}$ must be increased greatly to allow for closed orbits closer to the origin. However, as $\bar{x}$ is increased, the value of $U_\perp$ necessary to reach the origin also increases. Thus, at sufficiently small x, only exponentially few trajectories will be present that are still in quasi-closed orbits. Since the majority of ions are therefore far from their effective potential maximum, we may expand equation (93) in the limit of

$\chi(x, \bar{x}) - \chi(0, \bar{x}) \ll \chi_{\mathrm{M}}(\bar{x}) - \chi(0, \bar{x})$, giving

$$\Delta v_x - \Delta v_{x_0} = -\Delta \left[\frac{1}{v_{x_0}}\right] \delta\chi + \frac{1}{2}\Delta \left[\frac{1}{v_{x_0}^3}\right] \delta\chi^2 + O\left(\frac{\delta\chi^3}{v_{\mathrm{t,i}}^5}\right), \tag{95}$$

with

$$\Delta \left[\frac{1}{v_{x_0}^n}\right] = \frac{1}{\left(2\left(\chi_{\mathrm{M}}(\bar{x}) - \chi(0, \bar{x})\right)\right)^{\frac{n}{2}}} - \frac{1}{\left(2\left(\Delta_{\mathrm{M}} + \chi_{\mathrm{M}}(\bar{x}) - \chi(0, \bar{x})\right)\right)^{\frac{n}{2}}}. \tag{96}$$

Collecting what are now the lowest order terms in the quasineutrality equation gives

$$\begin{aligned}
\frac{\mathrm{d}n_{\mathrm{e}}}{\mathrm{d}\phi}\delta\phi &= -Z\Omega_{\mathrm{i}}x \int_{\bar{x}_{\mathrm{c}}}^{\infty} \Omega_{\mathrm{i}}^2 \bar{x}\,\mathrm{d}\bar{x} \int_{\chi_{\mathrm{M}}(\bar{x})}^{\infty} \frac{F_{\mathrm{cl}}(\mu, U)}{\sqrt{2\left(U - \chi_{\mathrm{M}}(\bar{x})\right)}} \Delta \left[\frac{1}{v_{x_0}}\right] \mathrm{d}U \\
&\quad + Z\frac{\Omega_{\mathrm{i}}}{B}\delta\phi \int_{\bar{x}_{\mathrm{c}}}^{\infty} \Omega_{\mathrm{i}}\,\mathrm{d}\bar{x} \int_{\chi_{\mathrm{M}}(\bar{x})}^{\infty} \frac{F_{\mathrm{cl}}(\mu, U)}{\sqrt{2\left(U - \chi_{\mathrm{M}}(\bar{x})\right)}} \Delta \left[\frac{1}{v_{x_0}}\right] \mathrm{d}U.
\end{aligned} \tag{97}$$

Where the $\mathrm{d}n_{\mathrm{e}}/\mathrm{d}\phi$ is evalutated at the entrance to the Debye sheath. This could be solved in the form $\delta\phi = qx$, but this solution would break our assumption that the potential has infinite gradient at the origin. Instead, the terms of order $\delta\phi$ must cancel. This cancellation gives the *marginal kinetic Bohm condition*, only slightly different from that derived in [15]

$$\left.\frac{\mathrm{d}n_{\mathrm{e}}}{\mathrm{d}\hat{\phi}}\right|_{x=0} = Zv_{\mathrm{B}}^2 \int_{\bar{x}_{\mathrm{c}}}^{\infty} \Omega_{\mathrm{i}}\,\mathrm{d}\bar{x} \int_{\chi_{\mathrm{M}}(\bar{x})}^{\infty} \frac{F_{\mathrm{cl}}(\mu, U)}{\sqrt{2\left(U - \chi_{\mathrm{M}}(\bar{x})\right)}} \Delta \left[\frac{1}{v_{x_0}}\right] \mathrm{d}U. \tag{98}$$

This recovers [15]'s kinetic Bohm condition in the limit of $\phi_{\mathrm{cut}} \to -\infty$. Furthermore, we may note that this condition can be recast in the following form

$$\left.\frac{\mathrm{d}n_{\mathrm{e}}}{\mathrm{d}\hat{\phi}}\right|_{x=0} = Zv_{\mathrm{B}}^2 \iiint \frac{f_{i,0}(\mathbf{v})}{v_x^2}\mathrm{d}\mathbf{v}, \tag{99}$$

by using the following identity

$$\begin{aligned}
&Zv_{\mathrm{B}}^2 \int_{\bar{x}_{\mathrm{c}}}^{\infty} \Omega_{\mathrm{i}}\,\mathrm{d}\bar{x} \int_{\chi_{\mathrm{M}}(\bar{x})}^{\infty} \frac{F_{\mathrm{cl}}(\mu, U)}{\sqrt{2\left(U - \chi_{\mathrm{M}}(\bar{x})\right)}} \Delta \left[\frac{1}{v_{x_0}}\right] \mathrm{d}U \\
&= Zv_{\mathrm{B}}^2 \int_{\bar{x}_{\mathrm{c}}}^{\infty} \Omega_{\mathrm{i}}\,\mathrm{d}\bar{x} \int_{\chi_{\mathrm{M}}(\bar{x})}^{\infty} \frac{F_{\mathrm{cl}}(\mu, U)}{\sqrt{2\left(U - \chi_{\mathrm{M}}(\bar{x})\right)}}\mathrm{d}U \int_{-\infty}^{0} \frac{1}{v_x^2}\hat{\Pi}\left(v_x, V_0 - \Delta v_{x_0}, V_0\right)\mathrm{d}v_x \\
&= Zv_{\mathrm{B}}^2 \iiint \frac{f_{i,0}(\mathbf{v})}{v_x^2}\mathrm{d}\mathbf{v}.
\end{aligned} \tag{100}$$

Here, the top hat function $\hat{\Pi}$ is defined by

$$\hat{\Pi}(v_x, v_1, v_2) = \begin{cases} 1 \text{ if } v_1 < v_x < v_2, \\ 0 \text{ otherwise.} \end{cases} \tag{101}$$

Equation (99) is analogous to equation (79) of [1]. We note that the kinetic Chodura and Bohm conditions (equations (86) and (99)) are both similar in form, as the kinetic Chodura condition demands that ions be entering the presheath on average above the Bohm speed while the kinetic Bohm condition says that the presheath must accelerate these ions in the x direction into the Debye sheath. However, the kinetic Chodura condition arises as a constraint on the boundary conditions (in this case the entrance ion distribution function) while the marginal kinetic Bohm condition is an analytical property of the solution to the magnetic presheath. We further note that, while the derivative of density with respect to potential plays a small role in the Kinetic Chodura condition, it can have a large impact on the marginal kinetic Bohm condition since, as we discussed in section 3.2, the derivative of the electron density with respect to potential at $x = 0$ will diverge as $\phi(0) \to \phi_{\text{cut}}$

$$\frac{\mathrm{d}n_e}{\mathrm{d}\hat{\phi}}\bigg|_{x=0} = \frac{2\pi T_e}{m_e} \int_0^\infty \Omega_e \mathrm{d}\mu \left[-\int_0^\infty \frac{\partial \langle f_e \rangle_\varphi}{\partial U} \left(\Omega_e \mu + \frac{\bar{v}_\parallel^2}{2} - \frac{\Omega_e}{B}\phi(0), \mu \right) \mathrm{d}\bar{v}_\parallel \right.$$

$$- \int_0^{\sqrt{2\frac{\Omega_e}{B}(\phi(0)-\phi_{\text{cut}})}} \frac{\partial \langle f_e \rangle_\varphi}{\partial U} \left(\Omega_e \mu + \frac{\bar{v}_\parallel^2}{2} - \frac{\Omega_e}{B}\phi(0), \mu \right) \mathrm{d}\bar{v}_\parallel \quad (102)$$

$$\left. + \frac{1}{\sqrt{2\frac{\Omega_e}{B}(\phi(0) - \phi_{\text{cut}})}} \langle f_e \rangle_\varphi \left(\Omega_e \mu - \frac{\Omega_e}{B}\phi_{\text{cut}}, \mu \right) \right].$$

This means that as $\phi(0) \to \phi_{\text{cut}}$ the marginal kinetic Bohm condition becomes weaker, in the sense that the divergence of $\mathrm{d}n_e/\mathrm{d}\hat{\phi}$ makes the ion distribution move into lower regions of v_x so the ions are being accelerated less strongly in agreement with figure 7b.

Despite giving important information about the distribution function at $x = 0$, the marginal kinetic Bohm condition does not tell us about the form of the potential. To find the true dependence of $\delta\phi$ on x, we must expand to a further order, keeping

(a) Potentials

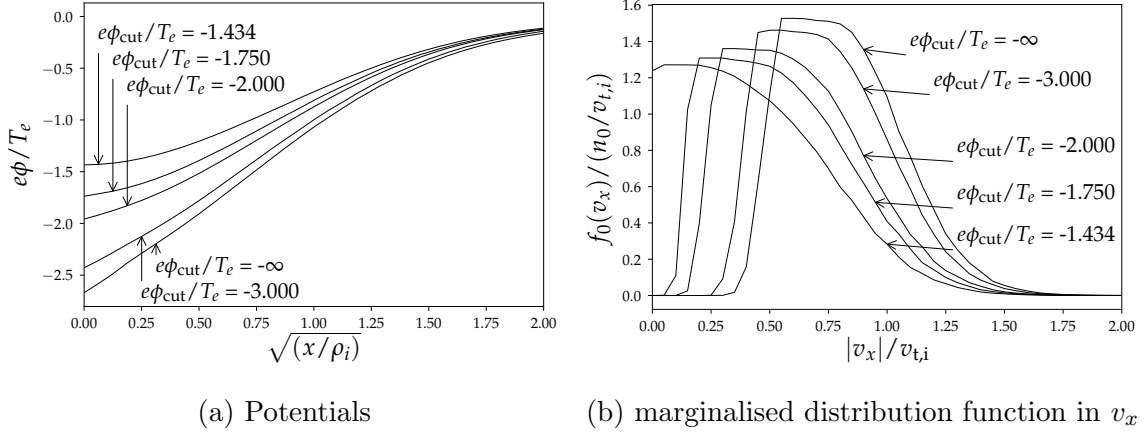(b) marginalised distribution function in v_x

Figure 7: Solutions to the electrostatic potential and the corresponding marginalised ion distribution function at the entrance to the Debye sheath for a range of cutoff potentials. Here $\alpha = 0.05$ and we have used the boundary conditions given in section 6 with $T_{\mathrm{e}} = T_{\mathrm{i}}$

only terms like $\delta\phi^2$ or x. Thus,

$$
\begin{aligned}
\frac{1}{2}\frac{\mathrm{d}^2 n_{\mathrm{e}}}{\mathrm{d}\phi^2}\delta\phi^2 = &-Z\Omega_{\mathrm{i}}x\int_{\bar{x}_{\mathrm{c}}}^{\infty}\Omega_{\mathrm{i}}^2\bar{x}\mathrm{d}\bar{x}\int_{\chi_{\mathrm{M}}(\bar{x})}^{\infty}\frac{F_{\mathrm{cl}}(\mu,U)}{\sqrt{2\left(U-\chi_{\mathrm{M}}(\bar{x})\right)}}\Delta\left[\frac{1}{v_{x_0}}\right]\mathrm{d}U \\
&+Z\frac{1}{2}\left(\frac{\Omega_{\mathrm{i}}\delta\phi}{B}\right)^2\int_{\bar{x}_{\mathrm{c}}}^{\infty}\Omega_{\mathrm{i}}\mathrm{d}\bar{x}\int_{\chi_{\mathrm{M}}(\bar{x})}^{\infty}\frac{F_{\mathrm{cl}}(\mu,U)}{\sqrt{2\left(U-\chi_{\mathrm{M}}(\bar{x})\right)}}\Delta\left[\frac{1}{v_{x_0}^3}\right]\mathrm{d}U,
\end{aligned}
\tag{103}
$$

and this is solved by

$$
\delta\phi = px^{\frac{1}{2}},
\tag{104}
$$

with p defined as

$$
p = \left[\frac{Z\int_{\bar{x}_{\mathrm{c}}}^{\infty}\Omega_{\mathrm{i}}^3\bar{x}\mathrm{d}\bar{x}\int_{\chi_{\mathrm{M}}(\bar{x})}^{\infty}\frac{F_{\mathrm{cl}}(\mu,U)}{\sqrt{2(U-\chi_{\mathrm{M}}(\bar{x}))}}\Delta\left[\frac{1}{v_{x_0}}\right]\mathrm{d}U}{\frac{1}{2}Zv_{\mathrm{B}}^4\int_{\bar{x}_{\mathrm{c}}}^{\infty}\Omega_{\mathrm{i}}\mathrm{d}\bar{x}\int_{\chi_{\mathrm{M}}(\bar{x})}^{\infty}\frac{F_{\mathrm{cl}}(\mu,U)}{\sqrt{2(U-\chi_{\mathrm{M}}(\bar{x}))}}\Delta\left[\frac{1}{v_{x_0}^3}\right]\mathrm{d}U-\frac{1}{2}\frac{\mathrm{d}^2 n_{\mathrm{e}}}{\mathrm{d}\hat{\phi}^2}}\right]^{\frac{1}{2}}.
\tag{105}
$$

Together with the modified kinetic Bohm condition given in equation (98), we may exhibit some important features of the factor p. First, in Appendix B we find a sufficient condition for p to be finite. This condition is

$$
\frac{3}{n_{\mathrm{e}}}\left(\frac{\mathrm{d}n_{\mathrm{e}}}{\mathrm{d}\phi}\right)^2 > \frac{\mathrm{d}^2 n_{\mathrm{e}}}{\mathrm{d}\phi^2},
\tag{106}
$$

where the derivatives are evaluated at $\phi(0)$. We further prove that the entrance distribution function we choose in section 6 satisfies this condition, and hence that we do not need to further expand the quasineutrality condition to compute the asymptotic behaviour of the potential at $x = 0$. We can further show that p tends to zero as $\phi(0) \to \phi_{\text{cut}}$. To see this, we differentiate equation (102) with respect to ϕ giving

$$
\begin{aligned}
\frac{\mathrm{d}^2 n_{\text{e}}}{\mathrm{d}\hat{\phi}^2}\bigg|_{x=0} = \frac{2\pi T_{\text{e}}^2}{m_{\text{e}}^2} \int_0^\infty \Omega_{\text{e}}\mathrm{d}\mu &\left[\int_0^\infty \frac{\partial^2 \langle f_{\text{e}} \rangle_\varphi}{\partial U^2} \left(\Omega_{\text{e}}\mu + \frac{\bar{v}_\parallel^2}{2} - \frac{\Omega_{\text{e}}}{B}\phi(0), \mu \right) \mathrm{d}\bar{v}_\parallel \right. \\
&+ \int_0^{\sqrt{2\frac{\Omega_{\text{e}}}{B}(\phi(0)-\phi_{\text{cut}})}} \frac{\partial^2 \langle f_{\text{e}} \rangle_\varphi}{\partial U^2} \left(\Omega_{\text{e}}\mu + \frac{\bar{v}_\parallel^2}{2} - \frac{\Omega_{\text{e}}}{B}\phi(0), \mu \right) \mathrm{d}\bar{v}_\parallel \\
&- \frac{1}{\sqrt{2\frac{\Omega_{\text{e}}}{B}(\phi(0) - \phi_{\text{cut}})}} \frac{\partial \langle f_{\text{e}} \rangle_\varphi}{\partial U} \left(\Omega_{\text{e}}\mu - \frac{\Omega_{\text{e}}}{B}\phi_{\text{cut}}, \mu \right) \\
&\left. - \frac{1}{\left(2\frac{\Omega_{\text{e}}}{B}(\phi(0) - \phi_{\text{cut}})\right)^{3/2}} \langle f_{\text{e}} \rangle_\varphi \left(\Omega_{\text{e}}\mu - \frac{\Omega_{\text{e}}}{B}\phi_{\text{cut}}, \mu \right) \right].
\end{aligned}
\tag{107}
$$

Provided the distribution function $\langle f_{\text{e}} \rangle_\varphi(\Omega_{\text{e}}\mu - \Omega_{\text{e}}\phi_{\text{cut}}/B, \mu)$ in non-zero for some range of μ, it is guaranteed that the first derivative of n_{e} with respect to ϕ (given in equation (102)) will diverge to $+\infty$ as $\phi(0) \to \phi_{\text{cut}}$ while the second derivative will diverge to $-\infty$. This implies that the denominator of p diverges like $1/(\phi(0) - \phi_{\text{cut}})^{3/2}$. While the numerator in the bracket in p will also diverge, it will diverge with the same divergence as the term in the marginal kinetic Bohm condition (98), since the additional presence of $\bar{x}$ does not change the form of the divergence. Thus the numerator diverges only as $1/(\phi(0) - \phi_{\text{cut}})^{1/2}$. It follows that p will tend to zero as $\phi(0)$ tends to ϕ_{cut}. Therefore, the divergence of the electric field vanishes as the magnitude of the potential drop across the Debye sheath decreases. This is in agreement with the numerical results shown in figure 7a which shows the weakening of the electric field as the magnitude of the potential drop in the Debye sheath is decreased. While the vanishing divergence of the electic field is consistent with the absence of the Debye sheath implied by $\phi(0) = \phi_{\text{cut}}$, it indicates the electron density must be expanded with more care in this regime. This is done in the following section.

4.2.2. $\phi(0) = \phi_{\mathrm{cut}}$. From equation (73), we see that when $\phi(0) = \phi_{\mathrm{cut}}$, it will no longer be possible to Taylor expand the electron density in $\delta\phi$ and instead we must expand in $\sqrt{\delta\phi}$,

$$n_{\mathrm{e}}(x) = n_{\mathrm{e}}(0) + \frac{\mathrm{d}n_{\mathrm{e}}(x)}{\mathrm{d}\sqrt{\delta\phi}}\sqrt{\delta\phi} + O\left(n_{\mathrm{e}}(0)\frac{e\delta\phi}{T_{\mathrm{e}}}\right). \tag{108}$$

Since the ion physics has remained unchanged, the only alteration to equation (94) is that now there is another term of size $\sqrt{\delta\phi}$ on the left hand side, giving the square root order quasineutrality equation

$$\sqrt{\frac{T_{\mathrm{e}}}{e}}\frac{\mathrm{d}n_{\mathrm{e}}(x)}{\mathrm{d}\sqrt{\delta\phi}}\sqrt{\frac{e\delta\phi}{T_{\mathrm{e}}}} = Z\int_{\bar{x}_{\mathrm{m,I}}}^{\infty}\sqrt{2\delta\chi}\Omega\mathrm{d}\bar{x}\int_{\chi_{\mathrm{M}}(\bar{x})}^{\infty}\frac{F_{\mathrm{cl}}(\mu,U)}{\sqrt{2\left(U-\chi_{\mathrm{M}}(\bar{x})\right)}}\mathrm{d}U. \tag{109}$$

Having assumed the potential to be finite at the origin, this equation is solved by a finite gradient in potential at $x = 0$. Therefore, we are motivated to (for sufficiently small x) rewrite $\delta\phi$ as $\phi'(0)x$. This makes equation (109) an implicit equation for $\bar{x}_{\mathrm{m,I}}$, related to the gradient at the origin through equation (49),

$$\frac{\mathrm{d}n_{\mathrm{e}}}{\mathrm{d}\sqrt{\hat{\delta\phi}}} = v_{B}Z\int_{\bar{x}_{\mathrm{m,I}}}^{\infty}\sqrt{2\left(\frac{\bar{x}}{\bar{x}_{\mathrm{m,I}}}-1\right)}\Omega\mathrm{d}\bar{x}\int_{\chi_{\mathrm{M}}(\bar{x})}^{\infty}\frac{F_{\mathrm{cl}}(\mu,U)}{\sqrt{2\left(U-\chi_{\mathrm{M}}(\bar{x})\right)}}\mathrm{d}U. \tag{110}$$

Thus, for $\phi_{\mathrm{cut}} = \phi(0)$, the electric field at the origin is finite and there exist type 1 closed orbits. The transition from a divergence electric field to a finite one can be seen clearly in figure 7a which confirms that the factor p is indeed vanishing.

5. The limits of hot and cold ion temperature

In section 4.2 we considered the distinction between the cases $\phi(0) = \phi_{\mathrm{cut}}$ and $\phi(0) > \phi_{\mathrm{cut}}$. Given that the cutoff potential is a parameter of the problem, it is natural to ask whether solutions exist for all ϕ_{cut} and whether they have $\phi(0) = \phi_{\mathrm{cut}}$ or $\phi(0) > \phi_{\mathrm{cut}}$. We can answer these questions by appealing to the hot ion theory developed in [23] and [16]. The hot ion theory models the limit $T_{\mathrm{e}} \ll T_{\mathrm{i}}$ in which the potential cannot substantially distort the ion orbits. In this section we will first show that, for hot ions, there exists a 'critical cutoff': a cutoff potential above which quasineutral solutions (that adhere to our constraints on the elecrostatic potential)

do not exist. At this critical cutoff, we find $\phi(0) = \phi_{\text{cut}}$, while for all solutions below this cutoff, we will have $\phi(0) > \phi_{\text{cut}}$.

The existence of critical cutoffs is not unique to hot ions and it is possible to show that they apply to all finite ion temperatures. For zero ion temperature, we prove that no critical cutoffs exist due to the lack of finite ion orbit widths. This has an important implication: fluid models of the magnetic presheath fail at very shallow magnetic field angles

5.1. The hot ion limit

As the ion temperature is increased, the distortion of ion orbits due to the potential becomes weaker. In the limit of a very large ion temperature, the effect of this is that the ion motion at lowest order becomes independent of the potential. This was investigated in [16] with the input ion distribution function

$$F_{\text{cl}}(U) = 2n_{\text{i},\infty} \left(\frac{m_{\text{i}}}{2\pi T_{\text{i}}} \right)^{\frac{3}{2}} \exp \left(-\frac{m_{\text{i}}U}{T_{\text{i}}} \right) \Theta(v_z), \tag{111}$$

where Θ is the Heaviside function,

$$\Theta(s) = \begin{cases} 1 \text{ for } s \geq 0, \\ 0 \text{ for } s < 0. \end{cases} \tag{112}$$

For an electric field negligible for the ions, it is purely the finite orbit sizes that result in the depletion of ions in the presheath. It was shown in [16] that the density at $x = 0$ is given by

$$n_{\text{i,op}}(0) = n_{\text{i},\infty} \frac{\Gamma^2(3/4)}{\pi} \sqrt{\alpha}, \tag{113}$$

where the gamma function $\Gamma(x)$ is defined by $\Gamma(x) = \int_0^\infty t^{x-1}e^{-t}\mathrm{d}t$. Note that equation (113) is predictably only a function of α. This is a manifestation of the fact that the ions are unaltered by the potential in the presheath.

Since the ion density is fixed regardless of potential, and the presheath is quasineutral, the potential will take the required value to make the electron density

equal to the ion density. The electron density at $x = 0$ is

$$
\begin{aligned}
n_{\mathrm{e}}(0) = 2\pi \int_0^\infty \Omega_{\mathrm{e}} \mathrm{d}\mu & \left[\int_0^\infty \langle f_e \rangle_\varphi \left(\Omega_{\mathrm{e}}\mu + \frac{\bar{v}_\parallel^2}{2} - \frac{\Omega_{\mathrm{e}}}{B}\phi(0), \mu \right) \mathrm{d}\bar{v}_\parallel \right. \\
& \left. + \int_0^{\sqrt{2\frac{\Omega_{\mathrm{e}}}{B}(\phi(0)-\phi_{\mathrm{cut}}-\Phi(\mu,\Delta\phi_{\mathrm{DS}}))}} \langle f_e \rangle_\varphi \left(\Omega_{\mathrm{e}}\mu + \frac{\bar{v}_\parallel^2}{2} - \frac{\Omega_{\mathrm{e}}}{B}\phi(0), \mu \right) \mathrm{d}\bar{v}_\parallel \right].
\end{aligned}
\tag{114}
$$

If $\Phi(\mu, \Delta\phi_{\mathrm{DS}})$ is neglected and the input electron distribution function is a decreasing function of energy, then the lower bound of equation (114) is reached when $\phi(0) = \phi_{\mathrm{cut}}$ (see figure 6). Assuming that this global minima is still present when $\Phi(\mu, \Delta\phi_{\mathrm{DS}}) \neq 0$, we denote the value of $n_{\mathrm{e}}(0)$ when $\phi(0) = \phi_{\mathrm{cut}}$ by $n_{\mathrm{e,min}}$,

$$
n_{\mathrm{e,min}}(\phi_{\mathrm{cut}}) = 2\pi \int_0^\infty \Omega_{\mathrm{e}} \mathrm{d}\mu \int_0^\infty \langle f_e \rangle_\varphi \left(\Omega_{\mathrm{e}}\mu + \frac{\bar{v}_\parallel^2}{2} - \frac{\Omega_{\mathrm{e}}}{B}\phi_{\mathrm{cut}}, \mu \right) \mathrm{d}\bar{v}_\parallel.
\tag{115}
$$

If $n_{\mathrm{e,min}}(\phi_{\mathrm{cut}}) < n_{\mathrm{i,op}}(0)$, then there is a quasineutral solution with $\phi(0) > \phi_{\mathrm{cut}}$ such that $n_{\mathrm{e}}(0) = n_{\mathrm{i,op}}(0)$. If $n_{\mathrm{e,min}}(\phi_{\mathrm{cut}}) = n_{\mathrm{i,op}}(0)$, this implies that the quasineutral solution has $\phi(0) = \phi_{\mathrm{cut}}$. For such critical solutions, the Debye sheath has collapsed as the wall potential is reached at $x = 0$ on the magnetic presheath scale. Noting that equation (115) increases to $n_{\mathrm{e},\infty}$ as ϕ_{cut} approaches zero, there is a 'critical cutoff' ϕ_{crit} for which $n_{\mathrm{e,min}}(\phi_{\mathrm{crit}}) = n_{\mathrm{i,op}}(0)$. For $\phi_{\mathrm{cut}} > \phi_{\mathrm{crit}}$, the electron density is constrained, sufficiently close to the wall, to be greater than the ion density and thus no quasineutral solutions can exist. Heuristically, the reason for the existence of the critical cutoffs is as follows. The electron density within the presheath is controlled entirely by the potential. A greater potential drop in the presheath results in more electrons being repelled and the density of electrons at $x = 0$ lowering. Raising the cutoff potential ϕ_{cut} limits the potential drop in the presheath and thus limits the minimum electron density as fewer electrons can be repelled. By raising the cutoff, the minimum electron density can be made arbitrarily close to the electron density far from the wall. The ion density however, is not only reduced by presence of an electric field but also by the finite width of the ion orbits. This finite width means that the density will reduce as we let $x \to 0$ as there is a smaller chance an ion could be found close to the wall without having previously touched the absorbing wall. Thus, the cutoff can be raised to a point where the minimum electron density is larger than the fixed ion density at $x = 0$ and, as a result, there can be no quasineutral

(a) Critical cutoffs
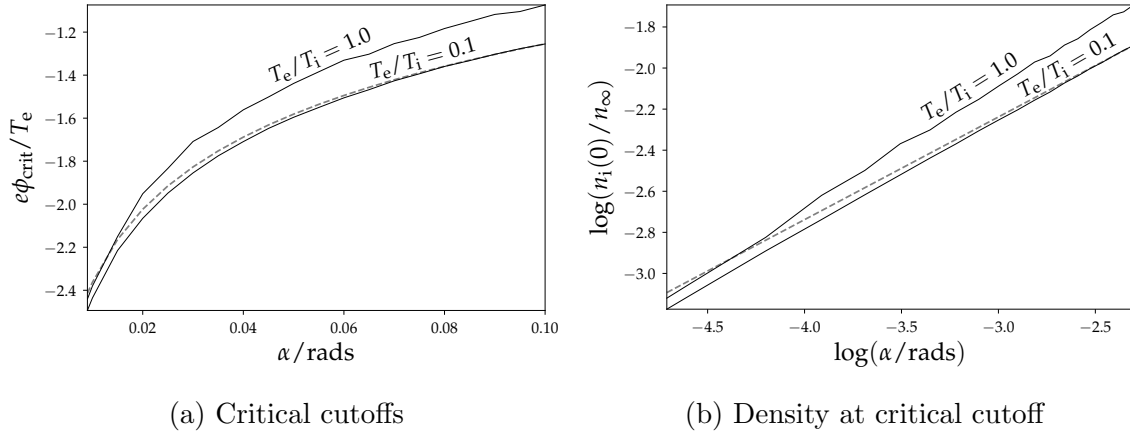
(b) Density at critical cutoff

Figure 8: Here we see the critical cutoffs as a function of α for two values of the temperature ratio with the boundary conditions specified in section 6. The dashed line represents the theoretical value of these quantities in the limit of hot ions.

solution within our assumption of a monotonic increasing potential profile. The critical cutoffs can be recovered numerically for finite $T_{\mathrm{e}}/T_{\mathrm{i}}$ (see section 6 for the numerical method). Figures 8a and 8b show the critical cutoffs as a function of α for two electron to ion temperature ratios. Even in the case of equal electron and ion temperatures, the solutions lie close to the theoretical hot ion limit of equation (113). This is a manifestation of the reduced distortion of the ion orbits near the wall due to the weaker electric field present in the critical solutions as these solutions are not longer forced to satisfy the marginal kinetic Bohm condition. In section 5.2 we show that this effect is indeed only present when modelling finite orbit widths, as modifying Chodura's fluid model does not give rise to any critical cutoffs.

5.2. The cold ion limit

In the limit of $T_{\mathrm{i}}/T_{\mathrm{e}} \to 0$, the ions can be considered mono-energetic upon entering the magnetic presheath. As such, the ions will follow a single trajectory. This means that the velocity of a given ion becomes a function of only its x position. This allows us to rewrite equations (14), (15) and (16) for the ions as equations for the fluid velocities u_x, u_y and u_z as a function of position

$$u_x \frac{\mathrm{d}u_x}{\mathrm{d}x} = -\frac{\Omega_{\mathrm{i}}}{B}\frac{\mathrm{d}\phi}{\mathrm{d}x} + \Omega_{\mathrm{i}}u_y \cos\alpha, \tag{116}$$

$$u_x \frac{\mathrm{d}u_y}{\mathrm{d}x} = -\Omega_i u_x \cos\alpha - \Omega_i u_z \sin\alpha, \tag{117}$$

and

$$u_x \frac{\mathrm{d}u_z}{\mathrm{d}x} = \Omega_i u_y \sin\alpha. \tag{118}$$

As well as this, we make use of the fluid continuity equation

$$\frac{\mathrm{d}}{\mathrm{d}x}(n_i u_x) = \frac{1}{Z}\frac{\mathrm{d}}{\mathrm{d}x}(n_e u_x) = 0. \tag{119}$$

Here, we have invoked quasineutrality in order to relate the flow equation to our much simpler equations involving the electron density. We can then integrate equation (119) to give

$$u_x(x) = \frac{n_{e,\infty} u_{x,\infty}}{n_e(\phi(x))}, \tag{120}$$

where we have further specified that the electron density is a function of only ϕ locally, as in equation (73). Using equation (116), we find an expression for the y directed velocity in terms of the potential and its first derivative,

$$u_y(x) = \frac{1}{\Omega_i \cos\alpha}\left(-\frac{n_{e,\infty}^2 u_{x,\infty}^2}{n_e^3}\frac{\mathrm{d}n_e}{\mathrm{d}\hat{\phi}} + \frac{ZT_e}{m_i}\right)\frac{\mathrm{d}\hat{\phi}}{\mathrm{d}x}. \tag{121}$$

This then allows us to integrate equation (118),

$$\begin{aligned}
u_z(x) - u_{z,\infty} &= \tan(\alpha)\left[u_x(x) - u_{x,\infty} + \frac{ZT_e}{m_i}\int_0^{\hat{\phi}(x)}\frac{1}{u_x(\hat{\phi})}\,\mathrm{d}\hat{\phi}\right] \\
&= \tan(\alpha)\left[u_x(x) - u_{x,\infty} + \frac{ZT_e}{n_{e,\infty}u_{x,\infty}m_i}\int_0^{\hat{\phi}(x)}n_e(\hat{\phi})\,\mathrm{d}\hat{\phi}\right].
\end{aligned} \tag{122}$$

We note that equation (121) is a function of the first derivative of ϕ. Together with the energy conservation equation (19), this allows us to write a first order ODE in ϕ,

$$\frac{\mathrm{d}\hat{\phi}}{\mathrm{d}x} = \frac{\Omega_i \cos\alpha}{v_B^2 - \frac{n_{e,\infty}^2 u_{x,\infty}^2}{n_e^3(\phi)}\frac{\mathrm{d}n_e}{\mathrm{d}\hat{\phi}}}\sqrt{u_\infty^2 - u_x^2(\hat{\phi}(x)) - u_z^2(\hat{\phi}(x)) - 2v_B^2\hat{\phi}}, \tag{123}$$

A salient property of this ODE is that the potential gradient need not be finite. Indeed, motivated by the discussion of the gradient in the general case, we see that

the infinite gradient should mark the transition from the quasineutral presheath into the Debye sheath. This occurs when

$$v_B^2 = u_{x,\infty}^2 \frac{n_{e,\infty}^2}{n_e^3(\phi)} \frac{\mathrm{d}n_e}{\mathrm{d}\hat{\phi}} \approx \alpha^2 u_{z,\infty}^2 \frac{n_{e,\infty}^2}{n_e^3(\phi)} \frac{\mathrm{d}n_e}{\mathrm{d}\hat{\phi}}, \tag{124}$$

which can be recast, using equation (120), as a Bohm-like condition, consistent with equation (99) on the ions entering the Debye sheath,

$$\frac{n_e(0)}{u_x(0)^2} = \frac{1}{v_B^2} \frac{\mathrm{d}n_e}{\mathrm{d}\hat{\phi}}. \tag{125}$$

In the case of Maxwellian electrons, equation (124) recovers the result of Chodura [11] for the potential drop across the magnetic presheath. Note that equation (124) has a solution for any α and ϕ_{cut}. For smaller α the density at the origin will reduce itself so as to solve the equation. Thus, lower α results in a more negative potential at the Debye sheath entrance as in [11,15]. In our electron model, there is a minimum density at the origin since the potential at the origin cannot be reduced below the cutoff potential. Yet, equation (124) still has solutions for all α because the derivative of the density with respect to potential can be made arbitrarily large by making $\phi(0)$ arbitrarily close to ϕ_{cut}, as can be deduced from equation (73) and was shown explicitly in section 4.2. Thus, unlike with the finite temperature ions, there is no critical cutoff.

Solutions exist for every ϕ_{cut} and α, implying that the fluid ion model will be unable to predict the collapse of the Debye sheath. This is in contradiction to the results of [28] where purely Boltzmann electrons were assumed. Physically, while the large circular orbits of the hot ions meant that the reduction in density was inevitable, the cold ions are influenced entirely by the electric field. Hence, if the cutoff potential is raised towards zero, the cold ions are accelerated less and the density remains high. Thus, there is no critical cutoff for cold ions. This explains why the critical cutoff is much higher for the colder ions in figure 9, since the cutoff must be raised much further before the finite orbit widths cause the electron density to exceed the ion density.

6. Numerical method

In the following section, we will outline how the numerical method used here differs from that used in reference [15]. We will first detail the entrance distribution
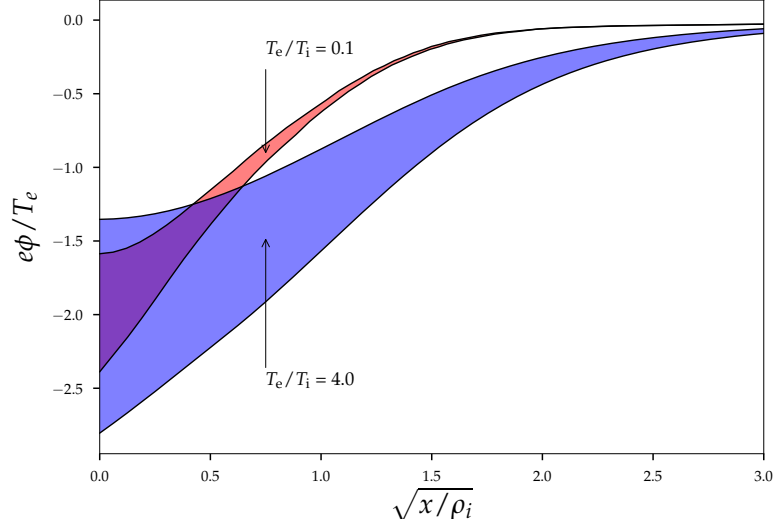
Figure 9: The difference between the critical potential solution (the upper lines) and the $\phi_{\text{cut}} \to -\infty$ potential solutions (the lower lines) for two different values of the temperature ratio using the boundary conditions detailing in section 6.

functions for electrons and ions. After this we will discuss the alterations to the iteration scheme necessary to handle solutions with cutoffs and to find the critical cutoffs.

6.1. Electron boundary conditions

In place of the Maxwellian electrons that were used by [14–16], our model accounts for the loss of electrons to the wall. Without a theory of the collisional presheath to provide an appropriate boundary condition on the electrons, the choice of entrance electron distribution functions is arbitrary, just as the original choice of a Maxwellian input was. We therefore choose a distribution function that will tend to the Maxwellian in the limit of $\phi_{\text{cut}} \to -\infty$: a truncated Maxwellian

$$f_{\text{e},\infty}(\mathbf{v}) = \frac{2}{1 + \text{erf}(\sqrt{-\frac{e}{T_{\text{e}}}\phi_{\text{cut}}})} \left(\frac{m_{\text{e}}}{2\pi T_{\text{e}}}\right)^{\frac{3}{2}} \exp\left(-\frac{m_{\text{e}}}{2T_{\text{e}}}|\mathbf{v}|^2\right) \Theta\left(\sqrt{-2\frac{\Omega_{\text{e}}\phi_{\text{cut}}}{B}} + v_{\parallel}\right),$$

$$(126)$$

where $\mathrm{erf}(x)$ is the error function defined by $\mathrm{erf}(x) = (2/\sqrt{\pi}) \int_0^x \exp(-u^2)\,\mathrm{d}u$. We have furthermore made the simplest choice of the function $\Phi(\mu, \Delta\phi_{\mathrm{DS}})$ as described in section 2.2, and set $\Phi(\mu, \Delta\phi_{\mathrm{DS}}) = 0$. In our conserved variables $\{U, \mu\}$, the distribution function is

$$f_{\mathrm{e}}(U, \mu) = \frac{2}{1 + \mathrm{erf}(\sqrt{-\frac{e}{T_{\mathrm{e}}}\phi_{\mathrm{cut}}})} \left(\frac{m_{\mathrm{e}}}{2\pi T_{\mathrm{e}}}\right)^{\frac{3}{2}} \exp\left(-\frac{m_{\mathrm{e}}}{T_{\mathrm{e}}}U\right). \tag{127}$$

Using equation (73) we arrive at the density as a function of $\phi(x)$ (see figure 6),

$$n_{\mathrm{e}}(x) = n_{\mathrm{e},\infty} \exp\left(\frac{e\phi(x)}{T_{\mathrm{e}}}\right) \frac{1 + \mathrm{erf}\left(\sqrt{\frac{e}{T_{\mathrm{e}}}(\phi(x) - \phi_{\mathrm{cut}})}\right)}{1 + \mathrm{erf}\left(\sqrt{-\frac{e}{T_{\mathrm{e}}}\phi_{\mathrm{cut}}}\right)}. \tag{128}$$

To allow for different possible electron distribution functions at the entrance of the presheath, instead of using equation (128), the code has the option to integrate the electron distribution function numerically using the procedure detailed in Appendix C. Since we have now included a cutoff potential, it is possible to calculate the electron current density along the magnetic field line. This is given by

$$J_e = \frac{v_{t,e}}{\sqrt{\pi}} \frac{n_{\mathrm{e},\infty}}{1 + \mathrm{erf}\left(\sqrt{-\frac{e\phi_{\mathrm{cut}}}{T_e}}\right)} \exp\left(\frac{e\phi_{\mathrm{cut}}}{T_e}\right). \tag{129}$$

This expression can also clearly be determined numerically for a general entrance electron distribution function.

6.2. Ion boundary conditions

As in [15, 16], without a scheme for determining the proper input distributions for the ions, there is an infinite number of possible distribution functions. We propose a family of possible distribution functions parametrised by $\tilde{\tau}$,

$$\tilde{\tau} = \frac{T_{\mathrm{i}}}{ZT_{\mathrm{e}}} \frac{1}{n_{\mathrm{e},\infty}} \frac{\mathrm{d}n_{\mathrm{e}}}{\mathrm{d}\hat{\phi}}\bigg|_{\hat{\phi}=0}. \tag{130}$$

This parameter deviates from $T_{\mathrm{i}}/ZT_{\mathrm{e}}$ by only a small amount, but we use this parameter as it is more convenient for the numerical handling of the kinetic Chodura

condition. Equipped with this, we choose identical input distributions functions to those chosen in [16],

$$
f_{i,\infty}(\mathbf{v}) = \begin{cases} \mathcal{N} n_{i,\infty} \frac{4v_z^2}{\pi^{3/2} v_{t,i}^5} \exp\left(-\frac{|\mathbf{v}-uv_{t,i}\hat{\mathbf{z}}|^2}{v_{t,i}^2}\right) \Theta(v_z) & \text{for } \tilde{\tau} \leq 1, \\ \mathcal{N} n_{i,\infty} \frac{4v_z^2}{\pi^{3/2} v_{t,i}^3 (v_{t,i}^2 + rv_z^2)} \exp\left(-\frac{|\mathbf{v}|^2}{v_{t,i}^2}\right) \Theta(v_z) & \text{for } \tilde{\tau} > 1. \end{cases}
\tag{131}
$$

In the conserved variables for the ions, this gives

$$
F(U,\mu) = \begin{cases} \mathcal{N} n_{i,\infty} \frac{8(U-\Omega_i\mu)}{\pi^{3/2} v_{t,i}^5} \exp\left[-\frac{2\Omega_i\mu + \left(\sqrt{2(U-\Omega_i\mu)}-uv_{t,i}\right)^2}{v_{t,i2}}\right] & \text{for } \tilde{\tau} \leq 1, \\ \mathcal{N} n_{i,\infty} \frac{8(U-\Omega_i\mu)}{\pi^{3/2} v_{t,i}^3 (v_{t,i}^2 + 2r(U-\Omega_i\mu))} \exp\left(-\frac{2U}{v_{t,i}^2}\right) & \text{for } \tilde{\tau} > 1. \end{cases}
\tag{132}
$$

The parameter $\mathcal{N}$ ensures that the distribution functions are normalised such that

$$
\iiint f_{i,\infty}(\mathbf{v}) \mathrm{d}\mathbf{v} = n_{i,\infty}.
\tag{133}
$$

The resulting value of $\mathcal{N}$ is

$$
\mathcal{N} = \begin{cases} \left[(1+2u^2)(1+\mathrm{erf}(u)) + \frac{2u}{\sqrt{\pi}}\exp(-u^2)\right]^{-1} & \text{for } \tilde{\tau} \leq 1, \\ r^{3/2}\left[2\sqrt{r} - 2\sqrt{\pi}\exp\left(\frac{1}{r}\right)\left(1-\mathrm{erf}\left(\frac{1}{\sqrt{r}}\right)\right)\right]^{-1} & \text{for } \tilde{\tau} > 1. \end{cases}
\tag{134}
$$

We motivated in section 4.1 that the entrance distribution function must at least satisfy the modified kinetic Chodura condition (86), and we further choose to marginally satisfy it. As such, we select the parameters u and r so that the distribution functions satisfy the modified Chodura equation (86). The resulting equations determining u and r are thus

$$
\mathcal{N}\left(1+\mathrm{erf}(u)\right) = \tilde{\tau}
\tag{135}
$$

for $\tilde{\tau} \leq 1$, and

$$
\frac{\mathcal{N}\sqrt{\pi}}{\sqrt{r}}\exp\left(\frac{1}{r}\right)\left(1-\mathrm{erf}\left(\frac{1}{\sqrt{r}}\right)\right) = \tilde{\tau}
\tag{136}
$$

for $\tilde{\tau} > 1$. The fluid velocity in the z direction of the distribution functions is then a function of u or r, respectively, and is given by

$$
\frac{u_{z,\infty}}{v_{t,i}} = \mathcal{N}\left[u(3+2u^2)(1+\mathrm{erf}(u)) + \frac{2}{\sqrt{\pi}}\exp(-u^2)(1+u^2)\right] \quad \text{for } \tilde{\tau} \leq 1
\tag{137}
$$

and

$$\frac{u_{z,\infty}}{v_{t,i}} = \frac{2\mathcal{N}}{r^2\sqrt{\pi}} \left(r - \exp\left(\frac{1}{r}\right) E_1\left(\frac{1}{r}\right) \right) \text{ for } \tilde{\tau} > 1, \tag{138}$$

where we have introduced the exponential integral

$$E_1(\xi) = \int_\xi^\infty \frac{\exp(-\eta)}{\eta} \, \mathrm{d}\eta. \tag{139}$$

6.3. The iteration scheme

The iteration procedure from [15] remains largely unchanged with the alteration of the electron model. We continue to use the numerical method detailed in [15] to calculate the ion density as a function of position for a given entrance ion distribution function and potential in the presheath. We discretise the presheath into a grid (x_n) in x and will calculate the potential and electron and ion densities at each x_n. Let $\phi_m(x_n)$ denote the potential at position x_n on the mth iteration. Likewise $n_{e,m}(x_n)$ and $n_{i,m}(x_n)$ will denote the electron and ion densities at position x_n on the mth iteration. We will see that there are steps in the iteration in which using the desired cutoff (denoted $\phi_{cut,desired}$) would produce an error. As such, the cutoff potential is also iterated and $\phi_{cut,m}$ will denote the cutoff at the mth iteration.

At each step in the iteration, we verify how close the system is to fulfilling quasineutrality condition (75), and we deem quasineutrality to be satisfied if

$$\left[\frac{1}{N+1} \sum_{\{x_n\}} \left(\frac{n_{i,m}(x_n)}{n_{e,m}(x_n)} - 1 \right)^2 \right]^{1/2} < \epsilon. \tag{140}$$

Here $N+1$ is the number of points in x_n, and ϵ was taken to be 0.007 for our numerical solution. The electron density is calculated from (73) using the numerical method detailed in Appendix C. For a given cutoff, this gives the electron density as a function of potential which we will denote $\tilde{n}_{e,\phi_{cut}}(\phi)$,

$$\tilde{n}_{e,\phi_{cut}} : [\phi_{cut}, 0] \to [n_{e,min}(\phi_{cut}), n_{e,\infty}]. \tag{141}$$

The electron density (128) is a monotonic increasing function of potential for the distribution functions we consider, as well as others. As a result, we can define an inverse function denoted by $\tilde{\phi}_{\phi_{cut}}(n)$,

$$\tilde{\phi}_{\phi_{cut}} : [n_{e,min}(\phi_{cut}), n_{e,\infty}] \to [\phi_{cut}, 0]. \tag{142}$$

We further define $\tilde{\phi}_{\text{cut}}(n_{\min})$ to be the inverse function of $n_{\text{e},\min}(\phi_{\text{cut}})$, defined in (115) (i.e. this returns the cutoff potential that would make $n_{\min}$ the minimum possible electron density in the presheath).

We may now present the iteration scheme. After specifying an initial potential profile $\phi_1(x_n)$ we begin the iteration:

(i) find $n_{\text{i},m}(x_n)$ from $\phi_m(x_n)$;

(ii) set $\phi_{\text{cut},m} = \min\left(\phi_m(0), \phi_{\text{cut,desired}}, \tilde{\phi}_{\text{cut}}(n_{\text{i},m}(0))\right)$;

(iii) set $n_{\text{e},m}(x_n) = \tilde{n}_{\text{e},\phi_{\text{cut},m}}(\phi_m(x_n))$;

(iv) stop the iteration if quasineutrality satisfies (140);

(v) set $\phi_{m+1}(x_n) = \tilde{\phi}_{\phi_{\text{cut},m}}\left(wn_{\text{e},m}(x_n) + (1-w)n_{\text{i},m}(x_n)\right)$;

(vi) update the entrance ion distribution function to ensure that the modified kinetic Chodura condition (86) is satisfied;

(vii) go to step (i).

Here w is a weight factor (which took values between 0.8 and 0) that quantifies how much the potential will change at each iteration step. After the first potential guess, each subsequent iteration is calculated by inverting the electron density relation on a weighted average of the electron and ion density. The procedure (i) used to calculate the ion density for a given potential $\phi_m(x_n)$ remains unchanged from [15]. The remainder of the procedure is devoted to finding the electron density and then inverting the weighted average of the densities to achieve the potential for the next iteration. This procedure is analogous to the one used in [15], but is now made more complicated by the presence of a cutoff potential. This is because the cutoff potential places a lower limit on both the electron density and the potential itself. If $\phi_m(x_n) < \phi_{\text{cut,desired}}$, then it would not be possible to find $n_{\text{e},m}(x_n)$ using $\tilde{n}_{\phi_{\text{cut,desired}}}$ since $\phi_m(x_n)$ would not be in the domain of $\tilde{n}_{\phi_{\text{cut,desired}}}$. Similarly, if the ion density is lower than the electron density, then the weighted density $wn_{\text{e},m}(x_n) + (1-w)n_{\text{i},m}(x_n)$ can be outside the domain of $\tilde{\phi}_{\phi_{\text{cut,desired}}}$ or $\tilde{\phi}_{\phi(0)}$, which would make step (v) impossible. Thus, in step (ii), we choose the cutoff to be the minimum of $\phi_m(0)$, $\phi_{\text{cut,desired}}$ and $\tilde{\phi}_{\text{cut}}(n_{\text{i},m}(0))$. For the majority of solutions, the iteration will terminate with $\phi_{\text{cut},m} = \phi_{\text{cut,desired}}$, indicating that a solution has been found at the required cutoff. However, it is possible for the iteration to terminate with $\phi_{\text{cut},m} = \phi_m(0) = \tilde{\phi}_{\text{cut}}(n_{\text{i},m}(0))$. These correspond to the critical cutoff solutions

discussed in section 4.2.2. It is also evident from the iteration scheme that setting the desired cutoff any higher will result in the same critical cutoff solution.

7. Results

Figure 7a shows the potential throughout the presheath for a range of cutoff potentials. By plotting this against $\sqrt{x}$, we see the linear dependence near the origin that characterises a diverging electric field at the entrance to the Debye sheath. This is what we predicted. As the cutoff potential is raised, the gradient of the potential with respect to $\sqrt{x}$ decreases. This corresponds to the factor p in equation (105) decreasing, which we predicted in section 4.2. Finally, when $\phi_{\text{cut}} = \phi(0)$, we see that the potential becomes quadratic in $\sqrt{x}$. Thus the divergence of the electric field vanishes along with the Debye sheath for this solution.

The shrinking of the region with diverging electric field is closely related to the weakening of the modified kinetic Bohm condition discussed in section 4.2.1. Figure 7b shows this directly by displaying the marginalised ion distribution function in v_x, $f_0(v_x) = \int f_i(x = 0, v_x, v_y, v_z) \mathrm{d}v_y \mathrm{d}v_z$, at the entrance to the Debye sheath ($x = 0$) for the same solutions displayed in figure 7a. For solutions with $\phi_{\text{cut}} \neq \phi(0)$, the distribution falls rapidly to zero as $v_x \to 0$ which is in agreement with equation (99). As the cutoff potential is raised towards the critical cutoff, we find the density of particles with low v_x increases. This is a manifestation of the electric field being weaker and ions being accelerated less strongly into the Debye sheath. Finally, when we reach the critical solution ($\phi_{\text{cut}} = \phi(0)$), there is a non-zero density of particles with $v_x = 0$, indicating that there are particles at a turning point as they reach $x = 0$, as was expected from section 4.2.2. In the nomenclature of section 2.3, this is equivalent to the statement that type 2 and type 1 orbits are present for solutions with $\phi_{\text{cut}} = \phi(0)$, whereas only type 2 orbits are present for solutions with $\phi(0) > \phi_{\text{cut}}$ (as type 1 orbits have turning points at $x = 0$).

Figure 5 shows the ion densities throughout the presheath for two solutions, one at the critical cutoff and one at $\phi_{\text{cut}} = -\infty$. The dashed and dotted lines show the closed and open orbit densities, respectively. In both cases, the ion densities drop significantly as we approach $x = 0$. However, there are qualitative differences between the two solutions. In solutions with $\phi(0) > \phi_{\text{cut}}$, there is a region near $x = 0$ where the closed orbit density becomes very close to zero and the open orbit density makes up almost the entire portion of the ion density. This is an identical

result to the one found in [15] and confirms that the open orbit density is necessary to correctly understand a kinetic treatment of the ions in the presheath. The steep gradients in the potential are causing all the closed orbits to be open before reaching the wall. Again, this can be phrased in the language of type 1 and type 2 orbits discussed in section 2.3: the steep gradient of the electric field makes all orbits type 2. Sufficiently close to $x = 0$, the only closed orbits that can be found are those with high energy on very large orbits (so that the restoring force of the magnetic field can compete with the large electric field) of which there are exponentially few. In contrast, when $\phi(0) = \phi_{\mathrm{cut}}$, the closed orbit density is linear near the origin. Closed orbits are present arbitrarily close to the wall.

A subtle but important feature of figure 5 which we have not discussed yet is the increase in open orbit density at the origin when going from the non-critical to critical regimes. Of particular importance is the change of scaling of this density with α. In [15, 23], it was shown that the density would scale proportionally with α in the shallow-angle limit for non-critical solutions. It was further demonstrated that, if there were a significant number of type 1 open orbits, the density would scale like $\sqrt{\alpha}$. This feature was not realisable outside of the hot ion theory (studied in [23]) as the diverging electric field did not permit type 1 orbits to exist. At the critical cutoff, however, the electric field is finite and no such limitations on type 1 orbits are present. Figure 8b shows the plot on logarithmic scales of density at the origin against magnetic field angle for two separate electron to ion temperature ratios. The solution with $T_{\mathrm{e}}/T_{\mathrm{i}} = 0.1$ lies close to the prediction made by the hot ion theory given in equation (113), although the agreement worsens as α is reduced since the approximation of section 5.1 that the ions are independent of the potential worsens as the presheath potential becomes more negative. The fact that the critical cutoff becomes more negative as α is decreased can be seen in figure 8a which shows the critical cutoffs as a function of α for the same two temperature ratios.

The existence of critical cutoffs, or equivalently maximum ion densities, presents a further interesting feature relating to the wall current. Raising the cutoff raises the electron current onto the wall, as fewer electrons are repelled when the potential is less negative. However, since the cutoff cannot be raised above the critical value, for each α there is a maximum electron current onto the wall. Using equation (129), we find that the maximum electron current density is [21]

$$J_{\mathrm{e,max}} = -e\frac{v_{\mathrm{t,e}}}{\sqrt{\pi}}n_{\mathrm{e,min}}(\phi_{\mathrm{crit}})\alpha. \tag{143}$$
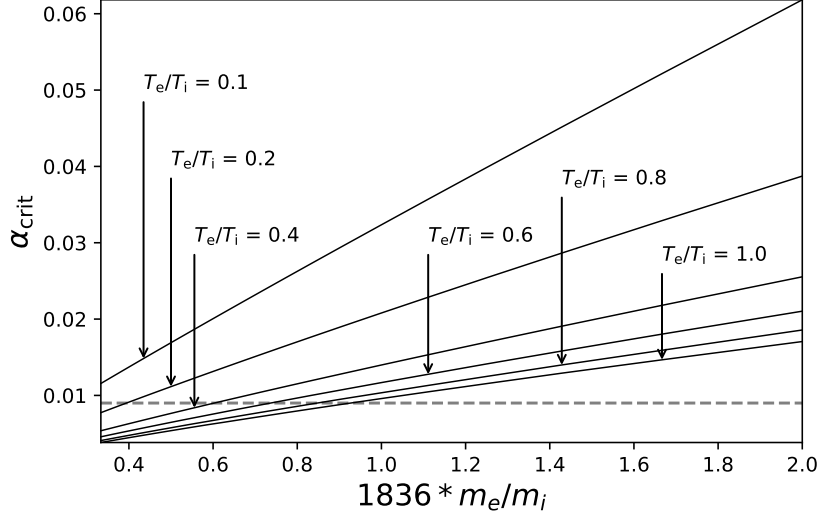
Figure 10: The value of α below which the ion current onto the wall will exceed the electron current as a function of the electron to ion mass ratio. The dashed line represents the lower limit in α that the code can solve numerically. Below this value of α the data has been extrapolated using a power law fit.

The ion current onto the wall is simply $Ze\alpha n_{i,\infty}u_{z,\infty}$, with $u_{z,\infty}$ given in equations (137-138), leading to the scaling of the ion current density

$$J_i = ZeAc_s n_{i,\infty}\alpha, \tag{144}$$

where A is some factor of order unity and $c_s = \sqrt{(ZT_e + T_i)/m_i}$ the characteristic ion speed. Noting that the maximum ion density falls with α, we see by quasineutrality that the maximum electron current is guaranteed to fall faster in α. There is therefore an α below which the maximum electron current cannot equal the ion current. At this α, if the system is driven to have zero total current, $\phi(0)$ is forced to equal ϕ_{cut} (to achieve maximum electron current) and the Debye sheath will collapse. Numerically, this value of α could be found by scanning through the critical cutoff solutions at different α and finding the solutions for which the total current is zero. Equivalently, and for ease of calculation, we find these α values by fitting the ion density at the critical cutoff (figure 8b) to a power law in α and solving $J_i = J_{\text{e,max}}$ for α. This critical angle is shown in figure 10 as a function of the electron to ion mass ratio.
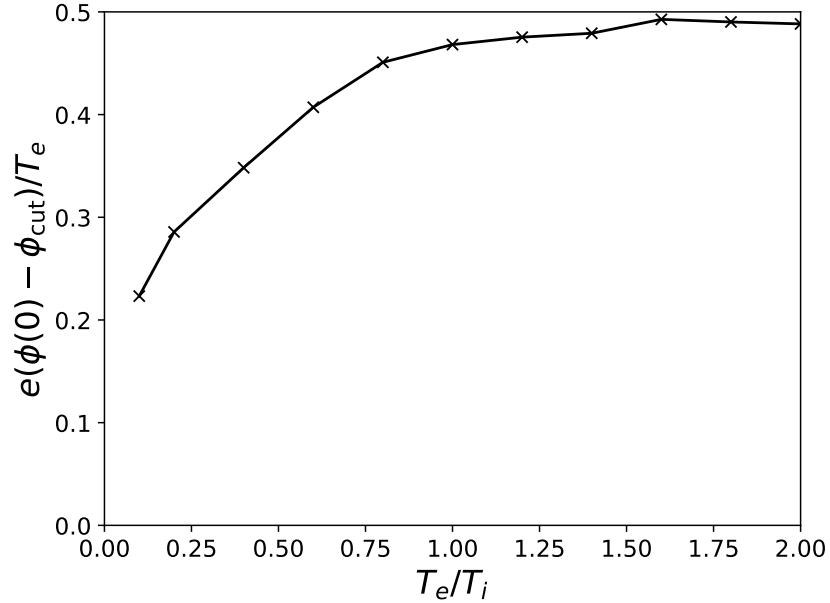
Figure 11: The values of the potential drop across the Debye sheath, $\phi(0) - \phi_{\mathrm{cut}}$ at $\alpha = 0.06$ ($\sim 3.4°$) for zero current solutions in the case of a Deuterium plasma. The potential drop in the Debye sheath accounts for between 10%-20% of the total potential drop, depending on the temperature ratio. Hence, the Debye sheath does not vanish at this angle.

The linear behaviour is exactly what would follow from a $\sqrt{\alpha}$ dependence of the density, predicted in [15], when type 1 orbits are present. Note that for a Deuterium plasma with equal ion and electron temperature, the critical angle for which the Debye sheath collapses in ambipolar conditions is 0.3-0.4 degrees. This is an order of magnitude smaller than previous estimates of about 3 degrees [28]. We show in figure 11 that the Debye sheath does not vanish at this angle for realistic values of the temperature ratio within our model.

8. Conclusion

We have extended the model of Geraldini et al [15] to account for the effects of absorption of electrons with sufficient energy to reach the wall. Drift kinetics was

used to find the kinetic equation satisfied by the electron distribution function. The density of electrons within our model was derived in equation (73), which we simplified by neglecting electron orbit size. The kinetic Bohm and Chodura conditions were derived in section 4, where we showed that the truncation of the electron distribution leads to subsonic sheaths, which agrees qualitatively with the results of [26]. It was shown in section 5.1 that the kinetic Bohm condition fully breaks down at a certain value of the wall potential, referred to as the critical cutoff. At this critical cutoff, the Debye sheath vanishes entirely, bringing the quasineutral presheath into direct contact with the wall. It was further shown in section 5.2 that a Chodura-like fluid theory cannot capture the existence of a critical cutoff due to the lack of finite ion orbit widths (equation (124)). The numerical method of Geraldini et al [15] was altered to include the revised electron model, and the existence of critical cutoffs for finite ion temperatures was shown. Finally, it was argued that, should the wall be at a floating potential, there is a critical magnetic field angle at which the cutoff potential is equal to the critical cutoff. At this point, no Debye sheath is present. Below this angle of incidence, or equivalently for a wall potential above the critical cutoff, the behaviour of the magnetic presheath and Debye sheath is unknown. The solution to the plasma wall boundary above the critical cutoff, therefore, must break one of the assumptions on the nature of our ion or electron model. The reversal of the sheath potential, $\phi_{\text{cut}} > \phi(0)$, which is excluded by our assumptions, is a possible scenario.

Acknowledgements

Appendix A. Derivation of the electron drift kinetic equation

From our definition (25) of φ

$$\sin \varphi = -\frac{v_y - v_E}{\sqrt{2\Omega_e \mu}}, \tag{A.1}$$

and

$$\cos \varphi = \frac{v_n}{\sqrt{2\Omega_e \mu}}. \tag{A.2}$$

The purpose of these expressions is to ensure we can write $\dot{\bar{x}}$, $\dot{\mu}$ and $\dot{\varphi}$ in terms of $\bar{x}$, μ and φ so that the gyroaverages can be computed trivially. We find

$$\begin{aligned}
\dot{\bar{x}} &= \dot{x} - \frac{\dot{v}_y}{\Omega_e} \\
&= -v_{\parallel} \sin \alpha + v_n (\cos \alpha - 1) \\
&= -v_{\parallel} \sin \alpha + \sqrt{2\Omega_e \mu}(\cos \alpha - 1) \cos \varphi,
\end{aligned} \tag{A.3}$$

$$\begin{aligned}
\dot{\mu} &= \frac{-\dot{v}_E (v_y - v_E)}{\Omega_e} \\
&= \frac{\sqrt{2\Omega_e \mu} \sin \varphi}{\Omega_e} \frac{1}{B} \frac{\mathrm{d}^2 \phi}{\mathrm{d}x^2}(x) \cos \alpha \left(v_n \cos \alpha - v_{\parallel} \sin \alpha \right),
\end{aligned} \tag{A.4}$$

and

$$\begin{aligned}
\dot{\varphi} + \Omega_e &= \frac{\dot{v}_E v_n}{2\Omega_e \mu} \\
&= \frac{\cos \varphi}{\sqrt{2\Omega_e \mu}} \frac{1}{B} \frac{\mathrm{d}^2 \phi}{\mathrm{d}x^2}(x) \cos \alpha \left(v_n \cos \alpha - v_{\parallel} \sin \alpha \right).
\end{aligned} \tag{A.5}$$

Appendix A.1. Gyroaverages

Here we calculate the gyroaverages of the quantities $\dot{\bar{x}}, \dot{\mu}$ and $\dot{\varphi}$. To do this we must rewrite equations (A.3), (A.4) and, (A.5) in terms of the variables that we hold constant for the gyroaverage, and φ. Since all our variables contain $v_{\parallel}$, it is first helpful to show that its φ dependence is small by a factor of m_e/m_i. We start by rewriting our equation for U

$$U = \Omega_e \mu - \frac{\Omega_e}{B} \phi(\bar{x}) + \frac{v_{\parallel}^2}{2} + v_E v_y - \frac{\Omega_e}{B} \frac{\mathrm{d}\phi}{\mathrm{d}x}(\bar{x})(x - \bar{x}) + O\left(v_{t,e} \frac{m_e}{m_i} \right). \tag{A.6}$$

Here we have Taylor expanded ϕ around $\bar{x}$ since we require our terms to be functions only of variables that we hold constant (this is a procedure that will be employed frequently in the gyroaveraging process). Now analysing the last three terms of equation (A.6), we have

$$
\begin{aligned}
v_y v_E - \frac{\Omega_e}{B} \frac{\mathrm{d}\phi}{\mathrm{d}x}(\bar{x})(x - \bar{x}) &= \frac{v_y}{B} \frac{\mathrm{d}^2\phi}{\mathrm{d}x^2}(\bar{x})(x - \bar{x}) + O\left(v_{t,e}^2 \frac{m_e}{m_i}\right) \\
&= O\left(v_{t,e}^2 \frac{m_e}{m_i}\right),
\end{aligned}
\tag{A.7}
$$

where, for the first equality, we have made use of equations (17) and (26), and we have Taylor expanded in the smallness of the electron gyroradius. Thus, inserting equation (A.7) back into equation (A.6), we see that

$$
v_\parallel = \sqrt{2\left(U - \Omega_e \mu + \frac{\Omega_e}{B}\phi(\bar{x})\right)} + O\left(v_{t,e} \frac{m_e}{m_i}\right).
\tag{A.8}
$$

Thus the gyrophase dependent part of $v_\parallel$ is order mass ratio smaller than the gyroaveraged piece, $\langle v_\parallel \rangle_\varphi$. From this and equations (A.3- A.5), we may now calculate the gyroaverages of our relevant variables.

$$
\langle \dot{\bar{x}} \rangle_\varphi = -\langle v_\parallel \rangle_\varphi \sin\alpha,
\tag{A.9}
$$

$$
\langle \dot{\mu} \rangle_\varphi = O\left(\frac{v_{t,e}^2}{\Omega_e} \frac{v_{t,e}}{\rho_i} \frac{m_e}{m_i} \alpha\right),
\tag{A.10}
$$

and

$$
\langle \dot{\varphi} + \Omega_e \rangle_\varphi = O\left(\frac{v_{t,e}}{\rho_i} \sqrt{\frac{m_e}{m_i}}\right).
\tag{A.11}
$$

We are now in a position where we can write down the lowest order gyroaveraged Vlasov equation

$$
\langle \mathcal{L}(\langle f_e \rangle_\varphi) \rangle_\varphi = -\sin\alpha \langle v_\parallel \rangle_\varphi \frac{\partial \langle f_e \rangle_\varphi}{\partial \bar{x}} + O\left(\frac{v_{t,e}}{\rho_i} \frac{m_e}{m_i} \alpha \langle f_e \rangle_\varphi\right).
\tag{A.12}
$$

Here the error in equation (A.12) comes from the term $\langle \dot{\mu} \rangle_\varphi \partial \langle f \rangle_\varphi / \partial\mu$.

Appendix A.2. First order correction $\langle \mathcal{L}(\tilde{f}_{\mathrm{e}}) \rangle_\varphi$

Here we will show that the term $\langle \mathcal{L}(\tilde{f}_{\mathrm{e}}) \rangle_\varphi$ can be safely neglected in equation (43), even in our small angle ordering (13). To do this we will show that the term scaling with $(m_{\mathrm{e}}/m_{\mathrm{i}})^{3/2}$ in $\langle \mathcal{L}(\tilde{f}_{\mathrm{e}}) \rangle_\varphi$ cancels, leaving terms that are smaller in mass ratio or that scale with α. First, we calculate the first order correction, $\tilde{f}_{\mathrm{e},1}$, by noting

$$\tilde{\dot{\mu}} = \frac{2\mu}{B} \frac{\mathrm{d}^2\phi}{\mathrm{d}x^2}(\bar{x}) \sin\varphi \cos\varphi + O\left(\frac{v_{\mathrm{t,e}}^2}{\Omega_{\mathrm{e}}} \frac{v_{\mathrm{t,e}}}{\rho_{\mathrm{i}}} \frac{m_{\mathrm{e}}}{m_{\mathrm{i}}} \right), \tag{A.13}$$

and

$$\tilde{\dot{\bar{x}}} = \left(v_\parallel - \langle v_\parallel \rangle_\varphi \right) \sin\alpha + \sqrt{2\Omega_{\mathrm{e}}\mu} \cos\varphi \left(\cos\alpha - 1 \right) = O\left(v_{\mathrm{t,e}} \frac{m_{\mathrm{e}}}{m_{\mathrm{i}}} \alpha, v_{\mathrm{t,e}} \alpha^2 \right). \tag{A.14}$$

Then solving equation (41) for $f_{\mathrm{e},1}$, we find

$$\tilde{f}_{\mathrm{e},1} = \frac{\mu}{\Omega_{\mathrm{e}} B} \left(\sin^2\varphi - \frac{1}{2} \right) \frac{\mathrm{d}^2\phi}{\mathrm{d}x^2} \frac{\partial \langle f_{\mathrm{e}} \rangle_\varphi}{\partial\mu} + O\left(\left(\frac{m_{\mathrm{e}}}{m_{\mathrm{i}}} \right)^{3/2} \langle f_{\mathrm{e}} \rangle_\varphi, \sqrt{\frac{m_{\mathrm{e}}}{m_{\mathrm{i}}}} \alpha^2 \langle f_{\mathrm{e}} \rangle_\varphi \right). \tag{A.15}$$

Now, calculating $\langle \mathcal{L}(\tilde{f}_{\mathrm{e},1}) \rangle_\varphi$ gives

$$\begin{aligned}
\langle \mathcal{L}(\tilde{f}_{\mathrm{e},1}) \rangle_\varphi &= -\frac{\mu}{2\Omega_{\mathrm{e}} B^2} \left(\frac{\mathrm{d}^2\phi}{\mathrm{d}x^2} \right)^2 \langle \sin 2\varphi \cos 2\varphi \rangle_\varphi \left[\frac{\partial \langle f_{\mathrm{e}} \rangle_\varphi}{\partial\mu} + \mu \frac{\partial^2 \langle f_{\mathrm{e}} \rangle_\varphi}{\partial\mu^2} \right] \\
&\quad + \langle \cos^3\varphi \sin\varphi \rangle_\varphi \frac{2\mu}{\Omega_{\mathrm{e}} B^2} \left(\frac{\mathrm{d}^2\phi}{\mathrm{d}x^2} \right)^2 \frac{\partial \langle f_{\mathrm{e}} \rangle_\varphi}{\partial\mu} \\
&\quad + O\left(\frac{v_{\mathrm{t,e}}}{\rho_{\mathrm{i}}} \langle f_{\mathrm{e}} \rangle_\varphi \left\{ \left(\frac{m_{\mathrm{e}}}{m_{\mathrm{i}}} \right)^2, \left(\frac{m_{\mathrm{e}}}{m_{\mathrm{i}}} \right)^{3/2} \alpha, \frac{m_{\mathrm{e}}}{m_{\mathrm{i}}} \alpha^2, \sqrt{\frac{m_{\mathrm{e}}}{m_{\mathrm{i}}}} \alpha^3 \right\} \right) \\
&= O\left(\frac{v_{\mathrm{t,e}}}{\rho_{\mathrm{i}}} \langle f_{\mathrm{e}} \rangle_\varphi \left\{ \left(\frac{m_{\mathrm{e}}}{m_{\mathrm{i}}} \right)^2, \sqrt{\frac{m_{\mathrm{e}}}{m_{\mathrm{i}}}} \alpha^3 \right\} \right),
\end{aligned} \tag{A.16}$$

where the largest terms have vanished upon gyroaveraging. Thus we have shown that the corrections due to the first order gyrophase dependent piece are sufficiently small and that equation (44) is still valid for our small α ordering (13).

Appendix B. Proof that p is finite

We will first show that p defined by equation (105) is finite for our boundary conditions defined in section 6. To do this we need only show that the denominator will always be non-zero. We rewrite the first term of the denominator as follows

$$
\begin{aligned}
Zv_{\mathrm{B}}^4 \int_{\bar{x}_{\mathrm{c}}}^{\infty} &\Omega_{\mathrm{i}} \mathrm{d}\bar{x} \int_{\chi_{\mathrm{M}}(\bar{x})}^{\infty} \frac{F_{\mathrm{cl}}(\mu, U)}{\sqrt{2\left(U - \chi_{\mathrm{M}}(\bar{x})\right)}} \Delta \left[\frac{1}{v_{x_0}^3}\right] \mathrm{d}U \\
&= Zv_{\mathrm{B}}^4 \int_{\bar{x}_{\mathrm{c}}}^{\infty} \Omega_{\mathrm{i}} \mathrm{d}\bar{x} \int_{\chi_{\mathrm{M}}(\bar{x})}^{\infty} \frac{F_{\mathrm{cl}}(\mu, U)}{\sqrt{2\left(U - \chi_{\mathrm{M}}(\bar{x})\right)}} \mathrm{d}U \int_{-\infty}^{0} \frac{3}{v_x^4} \hat{\Pi}\left(v_x, V_{\mathrm{op},0} - \Delta v_{x_0}, V_{\mathrm{op},0}\right) \mathrm{d}v_x \\
&= 3Zv_{\mathrm{B}}^4 \int \frac{f_{i,x,0}(v_x)}{v_x^4} \mathrm{d}v_x.
\end{aligned}
\tag{B.1}
$$

Hence it will be sufficient to prove that

$$
3Zv_{\mathrm{B}}^4 \int \frac{f_{i,x,0}(v_x)}{v_x^4} \mathrm{d}v_x > \frac{\mathrm{d}^2 n_{\mathrm{e}}}{\mathrm{d}\hat{\phi}^2}.
\tag{B.2}
$$

To do this we use the Bohm condition (equation (99)) and Schwarz's inequality to write

$$
\int \frac{f_{i,x,0}(v_x)}{v_x^4} \mathrm{d}v_x \geq \frac{\left(\int f_{i,x,0}(v_x) v_x^{-2} \mathrm{d}v_x\right)^2}{\int f_{i,x,0}(v_x) \mathrm{d}v_x} = \frac{1}{Zv_B^4} \frac{1}{n_{\mathrm{e}}(x)} \left(\frac{\mathrm{d}n_{\mathrm{e}}}{\mathrm{d}\hat{\phi}}\right)^2.
\tag{B.3}
$$

Since the inequality (B.3) is always true, if the inequality (106) holds then we are guaranteed to satisfy the inequality (B.2). Thus the inequality (106) is indeed a sufficient condition for p to be finite. Now specialising to our electron model with density described by (128), we may write the first derivative as

$$
\frac{\mathrm{d}n_{\mathrm{e}}}{\mathrm{d}\phi} = n_{\mathrm{e}}(\phi) + \frac{1}{\sqrt{\pi}} \frac{n_{\mathrm{e},\infty} e^{\hat{\phi}_{\mathrm{cut}}}}{1 + \mathrm{erf}\left(\sqrt{-\hat{\phi}_{\mathrm{cut}}}\right)} \frac{1}{\sqrt{\hat{\phi} - \hat{\phi}_{\mathrm{cut}}}} = n_{\mathrm{e}} + \tilde{A}(\phi),
\tag{B.4}
$$

and the second derivative as

$$
\frac{\mathrm{d}^2 n_{\mathrm{e}}}{\mathrm{d}\hat{\phi}^2} = \frac{\mathrm{d}n_{\mathrm{e}}}{\mathrm{d}\hat{\phi}} - \frac{1}{2\sqrt{\pi}} \frac{n_{\mathrm{e}} e^{\hat{\phi}_{\mathrm{cut}}}}{1 + \mathrm{erf}\left(\sqrt{-\hat{\phi}_{\mathrm{cut}}}\right)} \frac{1}{\left(\hat{\phi} - \hat{\phi}_{\mathrm{cut}}\right)^{3/2}} = \frac{\mathrm{d}n_{\mathrm{e}}}{\mathrm{d}\hat{\phi}} - \tilde{B}(\phi).
\tag{B.5}
$$

Here it is only relevant to know that $\tilde{A}$ and $\tilde{B}$ are positive functions of ϕ. Equation (B.5) then implies that the normalised second derivative of density is less than the normalised first derivative. We may the use equations (B.4) and (B.5) as well as the positivity of $\tilde{A}$ and $\tilde{B}$ to argue

$$\frac{1}{n_e}\left(\frac{\mathrm{d}n_e}{\mathrm{d}\hat{\phi}}\right)^2 = n_e + 2\tilde{A} + \frac{\tilde{A}^2}{n_e} > \frac{\mathrm{d}n_e}{\mathrm{d}\hat{\phi}} - \tilde{B} = \frac{\mathrm{d}^2 n_e}{\mathrm{d}\hat{\phi}^2}. \tag{B.6}$$

By combining our inequality (B.6) with our inequality (B.3), we see that we manifestly satisfy our sufficient inequality (106). Thus, p is finite for all solutions.

Appendix C. Integration scheme for the electron density

The electron density is given by equation (73). As such, we are concerned with integrals of the following form,

$$I = \int_{x=a}^{x=b} \mathrm{d}\left(\sqrt{x^2 - a^2}\right) g(x), \tag{C.1}$$

where x plays the role of $v_\parallel$. In the variable $z = \sqrt{x^2 - a^2}$, this integral would now admit the trapezium rule or Simpson's rule. One simply has to 'tile' the integration domain in z with tiles of width h. The complication is as follows: in our context $g(x)$ is the entrance distribution for the electrons and we anticipate situations where $g(x)$ will not be known exactly. Instead, if the entrance distribution function is supplied by a code, we expect $g(x)$ to be known only at certain values evenly spaced in x. We adapt Simpson's rule to work with evenly spaced x. This can be achieved as follows. For every small interval $[x_1, x_2]$, we use

$$\begin{aligned} I_{\text{strip}} &= \int_{x=x_1}^{x=x_2} \mathrm{d}\left(\sqrt{x^2 - a^2}\right) g(x) \\ &= \int_{x=x_1}^{x=x_2} \mathrm{d}\left(\sqrt{x^2 - a^2}\right) \left[g(x_1) + g'(x_1)(x-x_1) + \frac{g''(x_1)}{2}(x-x_1)^2 + O\left((x-x_1)^3\right)\right]. \end{aligned} \tag{C.2}$$

Rewriting x, we get

$$\begin{aligned} I_{\text{strip}} &= \int_{z=\sqrt{x_1^2-a^2}}^{z=\sqrt{x_2^2-a^2}} \mathrm{d}z \left[g(x_1) + g'(x_1)\left(\sqrt{z^2+a^2} - x_1\right)\right. \\ &\left. + \frac{g''(x_1)}{2}\left(\sqrt{z^2+a^2} - x_1\right)^2 + O\left((\sqrt{z^2+a^2} - x_1)^3\right)\right]. \end{aligned} \tag{C.3}$$

The terms involving square roots can be solved by hyperbolic substitution. This gives

$$
\begin{aligned}
I_{\text{strip}} = {}& \left(g(x_1) - x_1 g'(x_1) + \frac{x_1^2 + a^2}{2} g''(x_1) \right) \left[\sqrt{x_2^2 - a^2} - \sqrt{x_1^2 - a^2} \right] \\
& + \frac{(g'(x_1) - x_1 g''(x_1))}{2} \left[x_2 \sqrt{x_2^2 - a^2} - x_1 \sqrt{x_1^2 - a^2} + a^2 \left[\sinh^{-1} \left(\frac{\sqrt{x_2^2 - a^2}}{a} \right) \right. \right. \\
& \left. \left. - \sinh^{-1} \left(\frac{\sqrt{x_1^2 - a^2}}{a} \right) \right] \right] + \frac{g''(x_1)}{6} \left[(x_2^2 - a^2)^{3/2} - (x_1^2 - a^2)^{3/2} \right].
\end{aligned}
$$

$$(C.4)$$

Here, the first and second derivatives of the function are calculated using finite difference methods to the required level of accuracy

$$
g'(x_1) = \frac{g(x_1 + h) - g(x_1 - h)}{2h} + O(h^2) \tag{C.5}
$$

and

$$
g''(x_1) = \frac{g(x_1 + h) + g(x_1 - h) - 2g(x_1)}{h^2} + O(h). \tag{C.6}
$$

We will now address the size of the errors of our approximation to the integral. A common feature of strip based methods of integration is the scaling of the error with the strip size. Due to our choice of evenly spaced strips in x, however, the strips in z are not even. Therefore, we will split our discussion into one of regular strips in z with typical width $\sim h$ and irregular strips of width $\sim \sqrt{h}$. In both cases, the size of the neglected term is of order h^3 from two contributions: the truncation of the Taylor expansion of $g(x)$, and the finite difference expansion of the derivatives $g(x)$. There are an order unity number of irregular width strips so the total error from the irregular strips scales as $h^{7/2}$. There are of order $1/h$ regular strips of width h and therefore the total error of these strips scales like h^3.

References

[1] K-U Riemann. The Bohm criterion and sheath formation. *Journal of Physics D: Applied Physics*, 24(4):493, 1991.
[2] Noah Hershkowitz. Sheaths: More complicated than you think. *Physics of plasmas*, 12(5):055502, 2005.

[3] Scott D. Baalrud, Brett Scheiner, Benjamin Yee, Matthew M. Hopkins, and Edward Barnat. Interaction of biased electrodes and plasmas: Sheaths, double layers and fireballs. 2019.

[4] DE Hastings. A review of plasma interactions with spacecraft in low earth orbit. *Journal of Geophysical Research: Space Physics*, 100(A8):14457–14483, 1995.

[5] Jean-Pierre Boeuf. Tutorial: Physics and modeling of hall thrusters. *Journal of Applied Physics*, 121(1):011101, 2017.

[6] I H Hutchinson. Oblique ion collection in the drift approximation: How magnetized mach probes really work. *Physics of Plasmas (1994-present)*, 15(12):123503, 2008.

[7] I H Hutchinson. Principles of plasma diagnostics. *Plasma Physics and Controlled Fusion*, 44(12):2603, 2002.

[8] A Anders, S Anders, and I G Brown. Transport of vacuum arc plasmas through magnetic macroparticle filters. *Plasma Sources Science and Technology*, 4(1):1, 1995.

[9] P C Stangeby. The plasma boundary of magnetic fusion devices (IOP publishing, Bristol, UK). 2000.

[10] A Loarte, B Lipschultz, A S Kukushkin, G F Matthews, P C Stangeby, N Asakura, G F Counsell, G Federici, A Kallenbach, K Krieger, A Mahdavi, V Philipps, D Reiter, J Roth, J Strachan, D Whyte, R Doerner, T Eich, W Fundamenski, A Herrmann, M Fenstermacher, P Ghendrih, M Groth, A Kirschner, S Konoshima, B LaBombard, P Lang, A W Leonard, P Monier-Garbet, R Neu, H Pacher, B Pegourie, R A Pitts, S Takamura, J Terry, E Tsitrone, the ITPA Scrape-off Layer, and Divertor Physics Topical Group. Chapter 4: Power and particle control. *Nuclear Fusion*, 47(6):S203, 2007.

[11] R Chodura. Plasma–wall transition in an oblique magnetic field. *Physics of Fluids (1958-1988)*, 25(9):1628–1633, 1982.

[12] K-U Riemann. Theory of the collisional presheath in an oblique magnetic field. *Physics of Plasmas (1994-present)*, 1(3):552–558, 1994.

[13] D Bohm. *The Characteristics of Electrical Discharges in Magnetic Fields*, page 77, 1949.

[14] A Geraldini, F I Parra, and F Militello. Gyrokinetic treatment of a grazing angle magnetic presheath. *Plasma Physics and Controlled Fusion*, 59(2):025015, 2017.

[15] A Geraldini, F I Parra, and F Militello. Solution to a collisionless shallow-angle magnetic presheath with kinetic ions. *Plasma Physics and Controlled Fusion*, 60(12):125002, 2018.

[16] A Geraldini, F I Parra, and F Militello. Dependence on ion temperature of shallow-angle magnetic presheaths with adiabatic electrons. *Journal of Plasma Physics*, 85(6), 2019.

[17] D Tskhakaya and S Kuhn. Particle-in-cell simulations of the plasma-wall transition with a magnetic field almost parallel to the wall. *Journal of nuclear materials*, 313:1119–1122, 2003.

[18] D Tskhakaya and S Kuhn. The magnetised plasma-wall transition: Theory and PIC simulation. *Contributions to Plasma Physics*, 44(5-6):564–570, 2004.

[19] D Tskhakaya. One-dimensional plasma sheath model in front of the divertor plates. *Plasma Physics and Controlled Fusion*, 59(11):114001, 2017.

[20] D Coulette and G Manfredi. An Eulerian Vlasov code for plasma-wall interactions. *Journal of Physics: Conference Series*, 561(1):012005, 2014.

[21] D Coulette and G Manfredi. Kinetic simulations of the chodura and debye sheaths for magnetic

fields with grazing incidence. *Plasma Physics and Controlled Fusion*, 58(2):025008, 2016.

[22] U Daybelge and B Bein. Electric sheath between a metal surface and a magnetized plasma. *Physics of Fluids (1958-1988)*, 24(6):1190–1194, 1981.

[23] R H Cohen and D D Ryutov. Particle trajectories in a sheath in a strongly tilted magnetic field. *Physics of Plasmas (1994-present)*, 5(3):808–817, 1998.

[24] H A Claaßen and H Gerhauser. Ion gyro-cooling in the magnetic presheath. *Contributions to Plasma Physics*, 36(2-3):381–385, 1996.

[25] J H Ingold. Two-fluid theory of the positive column of a gas discharge. *Physics of Fluids (1958-1988)*, 15(1):75–85, 1972.

[26] Joaquim Loizu, Paolo Ricci, and Christian Theiler. Existence of subsonic plasma sheaths. *Physical Review E*, 83(1):016406, 2011.

[27] G Kawamura and A Fukuyama. Kinetic modeling of a sheath layer in a magnetized collisionless plasma. *Physics of Plasmas*, 14(8):083502, 2007.

[28] P C Stangeby. The chodura sheath for angles of a few degrees between the magnetic field and the surface of divertor targets and limiters. *Nuclear Fusion*, 52(8):083012, 2012.

[29] R. D. Hazeltine. Recursive derivation of drift-kinetic equation. *Plasma Physics*, 15(1), 1973.